



HAL
open science

Experimental study of rheological behavior of foam flow in capillary tubes

Sagyn Omirbekov, Hossein Davarzani, Bexultan Sabyrbay, Stéfan Colombano,
Azita Ahmadi-Senichault

► **To cite this version:**

Sagyn Omirbekov, Hossein Davarzani, Bexultan Sabyrbay, Stéfan Colombano, Azita Ahmadi-Senichault. Experimental study of rheological behavior of foam flow in capillary tubes. *Journal of Non-Newtonian Fluid Mechanics*, 2022, 302, pp.104774. 10.1016/j.jnnfm.2022.104774 . hal-03595052

HAL Id: hal-03595052

<https://hal.science/hal-03595052>

Submitted on 3 Mar 2022

HAL is a multi-disciplinary open access archive for the deposit and dissemination of scientific research documents, whether they are published or not. The documents may come from teaching and research institutions in France or abroad, or from public or private research centers.

L'archive ouverte pluridisciplinaire **HAL**, est destinée au dépôt et à la diffusion de documents scientifiques de niveau recherche, publiés ou non, émanant des établissements d'enseignement et de recherche français ou étrangers, des laboratoires publics ou privés.

Experimental study of rheological behavior of foam flow in capillary tubes

Sagyn Omirbekov^{a,b}, Hossein Davarzani^{a,*}, Bexultan Sabyrbay^a, Stéfán Colombano^a, Azita Ahmadi-Senichault^b

^a BRGM (French Geological Survey), 3 Avenue Claude Guillemin, Orléans 45100, France

^b Institut de Mécanique et Ingénierie de Bordeaux (I2M, TREFLE), Arts et Métiers ParisTech, Talence 33405, France

A B S T R A C T

Studies of foam flow in highly permeable porous media are still limited due to foam's complex behavior and discrepancies in foam research. Specifically, it is still unclear how foam flows in capillary tubes and what the effects of material and tube diameter are. We have investigated the rheology of pre-generated foam in capillary tubes. Experiments were carried out using two types of capillary tubes: hydrophobic (PTFE – polytetrafluoroethylene; FEP – fluorinated ethylene propylene) and hydrophilic (GT – glass tubes). The foam was previously formed in the sand-pack by co-injecting a surfactant solution and nitrogen gas. We investigated the effect of material and tube size on foam rheology versus gas fraction (for a fixed flow rate) and flow rate (for a fixed gas fraction). A three-parameter Herschel-Bulkley model was used to describe foam rheology in capillary tubes. Pictures of foam flow in GT and FEP tubes were taken to determine the mean bubble area using image analysis. We estimated wall-slip velocity in capillary tubes and compared the results with the bulk-foam rheology using an analytical expression of the Herschel-Bulkley model for volumetric flow through the circular tubes. We observed shear-thinning behavior in all capillary tubes (FEP, PTFE, GT), and the Herschel-Bulkley model successfully fitted its behavior. The foam in PTFE tubes behaved as a yield-stress fluid, while yield stress was not observed in GT and FEP tubes. We also found that transition foam quality depends on the material type and tube diameter. The results show that foam's apparent viscosity is higher in hydrophobic tubes (FEP and PTFE tubes) than in hydrophilic glass tubes. This was explained by the wall-slip velocity being higher in glass tubes than in FEP and PTFE tubes because of the difference in surface roughness. The corrected flow rate without wall slip matches the flow rate calculated using the measured bulk foam viscosity better. Therefore we conclude that considering wall-slip velocity is important when studying foam flow in porous media.

1. Introduction

Aqueous foam is a complex two-phase fluid that is a dispersion of gas-phase (bubbles) in a continuous liquid phase, where the thin liquid films are called lamellae. The liquid phase is commonly an aqueous surfactant suspension that plays a significant role in stabilizing the bubbles' lamellae.

Foams are used in many industries, for instance, in cosmetics, pharmaceuticals, food production, as insulating material in construction, and as a fire-fighting fluid. Foam is also widely used in the oil industry as a drilling fluid, especially as a fluid to extract oil through enhanced-oil recovery (EOR) methods [2,39]. Recently, foam has also been used in remediation efforts for polluted soil [33,42]. Since foam has a low density and a sizeable interfacial surface area, it can boost active contact with contaminants and help remove pollutants [66].

Foam in porous media can be formed by three underlying mechanisms: capillary snap-off, lamella division, and leave-behind [37]. However, strong foam cannot be generated in situ in very highly permeable porous media such as gravels because of the immense size of the pores, leading to low capillary pressures. This is often the case in highly permeable aquifers [1,3,44]. Using pre-generated foam to remediate contaminated aquifers is also not straightforward because of the surfactant dilution and flushing in groundwater that can inhibit further foam formation [14]. Therefore, pre-generated foam must be very stable in aquifers to avoid foam flushing and destruction.

Studying foam flow in porous media is challenging because foam has complex rheology and porous media has a highly complicated microstructure. For instance, [44] studied the behavior of pre-generated foam in highly permeable porous media. They found that foam behaves like a yield-stress fluid when its bubbles are smaller than pores. They also

Corresponding author

E-mail address: h.davarzani@brgm.fr (H. Davarzani).

observed that the apparent viscosity increases with permeability. This phenomenon was attributed to the ratio of bubbles to pore size. However, these internal details cannot be seen in porous media due to their very complicated structure. Recently, [45] also showed how complex foam rheology is. They compared the apparent foam viscosity in a porous medium to the bulk foam rheology, where the foams were pre-generated with the same sand-pack in both cases. They found that the apparent foam viscosity is higher than bulk foam viscosity, and this could be related to the complexity of foam flow in porous media such as a compressibility effect.

To simplify these circumstances, porous media geometry has been dramatically simplified in much research, where it is considered as a bundle of capillaries [9,20,52]. Capillary tubes have also been considered as the fundamental element used in the more sophisticated pore-network modeling approaches [57,67]. Therefore, we thoroughly explored foam flow in a capillary tube. That simple geometry allows us to address various inter-related aspects of foam behavior, namely rheology, stability, and bubble size. For instance, foam instability can be caused by bubble coalescence, drainage, and gas diffusion from small to large bubbles (Ostwald ripening), leading to a change in bubble size [65]. Therefore, we must study how foam flows in light of these aspects. Although the description of foam in porous media is based on insights on foam in tubes [32], the rheology in smooth capillaries is not directly representative of the expected behavior in geological porous media due, in particular, to the complex microstructure with pore bodies and throats [57]. For instance, in porous geological media such as aquifers, foam bubbles are expected to be the same size or larger than pores since gas diffusion from small to big bubbles brings this result. This can also be observed in bulk foams given sufficient time, and there is no end to this coarsening until only one giant bubble remains. Foam in a subsurface application certainly has many hours to coarsen to pore size. Therefore, an experiment with the residence time of a minute or less does not represent bubble sizes relative to tube size that would be seen in an application to subsurface porous media. Variations in pore body and throat diameters also affect foam flow in the porous medium. Because of the capillary resistance of films leaving the pore channels, most of the gas can be trapped in place, resulting in apparent yield stress. Hence, wall slip velocity is expected to be larger in porous media than in capillary tubes, since it depends on capillary pressure which is likely to be larger in porous media. Foam rheology in smooth capillaries is not representative of behavior in porous geological media. Geological porous media are also different from tubes in which water and gas are not forced to flow through the same pores. Therefore, foam with lower quality (i.e., bubbly liquid) would not occur in porous media, where the excess water would have found other flow paths due to capillary effects and gravity segregation.

The rheology of foam in tubes is often described as shear-thinning with and without yield stress. Several models were used to represent foam flow: the Bingham model [35], the power-law model [21,25], and the Herschel-Bulkley model [6,27,31]. For instance, David and Marsden [15] studied foam flow in glass tubes with diameters of 0.4, 0.6, 0.7, and 0.8 mm. They found the shear-thinning foam behavior with very low yield stress. Also, they corrected apparent foam viscosity by taking into account wall-slip velocity. Bretherton [5] studied a single bubble in smooth capillary glass tubes of 1 mm diameter, where he derived an expression for dynamic pressure drop in the bubble with constant surface tension. He also predicted bubble profile and bubble rise rate in a vertical tube with some assumptions. Hirasaki and Lawson [32] extended Bretherton's [5] results by investigating a chain of bubbles separated with lamellae. Hirasaki and Lawson [32] described the apparent viscosity of foam flow in smooth capillary tubes based on the Hagen-Poiseuille law. The generated foams with a gas fraction (f_g , foam quality) of 70% and above flowed through glass capillaries with radii of 0.1, 0.2, 0.25, 1, and 2.5 mm. The smallest bubble was equivalent to the size of the smallest capillary tube. They observed shear-thinning behavior for foam flowing in the tubes and described the apparent

foam viscosity by three main affecting factors: 1) liquid slugs between gas bubbles; 2) bubble shape deforming due to viscous and capillary forces; 3) the surface tension gradient, which was explained by accumulating active surface material at the back of the bubbles. They also noted that apparent foam viscosity depends on bubble size (texture), capillary radius, and gas fraction in foam. However, changing the length of the capillary tubes did not affect the foam behavior in those tubes. Cantant et al [8]. studied the rheology of foam through a small 200 mm long plexiglass channel with a cross-section of 3 mm by 9 mm. They found power-law behavior in foam flow with an exponential 2/3 dependence between the bubble velocity and pressure relation for complex foam structures, thus expanding Bretherton's [5] work. Herzhaft et al [31]. studied a pre-generated foam in a recirculating pipe rheometer made of two parallel stainless-steel pipes with an internal diameter of 7.7 and 10.9 mm. The foam's flow was examined with respect to its quality, varying from 20% to 85% for different surfactant concentrations and at various static pressures. They found Newtonian and yield stress-type behavior for low ($f_g \leq 50\%$) and high quality ($f_g \geq 60\%$) foams, respectively. Denkov et al [16]. studied foam rheology with foam quality of 90% using a rheometer. The foam was formed using a syringe with a needle id (inner diameter) of 2.5 mm. They found shear-thinning foam flow behavior. Denkov et al [17]. investigated surfactant effects, and bubble surfaces on bulk foam rheology where the foam quality $\geq 80\%$. They classified the rheological foam behavior into two different types: i) the results with power-law index, $n \approx 0.5$ referred to a first type system that corresponded to friction dominance in foam films; ii) the outcomes with $n < 0.5$ (mostly between 0.2 and 0.25) was defined as systems with essential energy dissipation on the bubble surfaces. Bogdanovic et al [4]. investigated the rheological behavior of foams with foam quality ranging from 86.2% to 99.6% in horizontal stainless-steel pipes with a diameter of 0.5 and 1 inch (corresponding to 12.7 and 25.4 mm respectively). The foam was generated by co-injection of nitrogen and a surfactant solution using a filter (50 μm or 90 μm opening size). They examined five different surfactants with three concentrations. They found that surfactant type impacted transition foam quality (f_g^*), where higher values were found for more stable foams. However, the change in pipe diameter did not significantly change the transition foam quality. They also observed shear-thickening foam flow behavior in high-quality regimes ($f_g > f_g^*$) in all experiments. In low-quality regimes ($f_g < f_g^*$), foams mostly behaved as a shear-thickening fluid in the 0.5 inch diameter pipe. However, in the 1 inch pipe, foams showed nearly Newtonian (slightly shear-thinning) behavior. Gajbhiye and Kam [23] conducted foam-flow experiments in stainless steel and nylon pipes. The flow was studied through pressure drop measurement and visually by filming the foam bubbles, since the nylon pipes were transparent. They pointed out that foam has shear-thickening flow behavior in the low-quality regime, indicated the effect of surfactant on the transition foam quality, and showed a schematic of two flow regimes observed based on the foam texture during the experiments. The high-quality regime was described by fine-textured foams and showed slug flow. In contrast, foam flow in the low-quality regime was characterized by stable flow of uniform foam and illustrated by either segregated or plug flow.

Gumati and Takahshi [26] studied experimentally how pre-generated foam flows through glass-bead packing in a 5 m long acrylic pipe with a 50 mm diameter. They found shear-thinning behavior for foams with a quality of 80%, 85%, and 95%, in which shear stress was determined to be a power-law function with the power-law index n respectively equal to 0.44, 0.45, and 0.42. Moreover, Du et al [19]. found the power-law behavior of foam flow in a glass tube with a 5 mm diameter.

From this review, we noticed that foams behave differently in tubes, and that contradictions among the various research studies may depend on the type of surfactant and gas, as well as on the medium in which foam flows. Another essential feature of foam flow in tubes is the wall-

slip velocity, which depends on the type of tube material, its surface roughness, diameter and depends critically on the thickness of the water film along the tube walls, along with the other factors [18,32]. The thickness of the water film is not simply a direct function of tube material but depends on velocity as well. This slip velocity is useful as a macro-scale description of the wall's boundary condition. The slip mechanism at the pore scale depends on a thin layer of liquid that does not slip but wets the wall and lubricates the foam flow. Therefore, when the foam is sheared, a large velocity gradient appears in this liquid layer. This low viscosity liquid leads to the foam slipping. Its existence was found in most foam studies through pipes. For example, Jastrzebski [34] assumed wall-slip velocity to be inversely proportional to pipe diameter during flow of concentrated suspensions. Harris and Reidenbach [28] observed no wall-slip velocity for foam flow in their 3 m high-temperature, high-pressure recirculating loop viscometer with a diameter of 7.75 mm. Thondavadi and Lemlich [62] found wall-slip velocity for foam flow in acrylic (Perspex) pipes. However, they did not observe wall-slip in galvanized-steel pipes (with roughness 100-500 μm). They noted that foam's acrylic surface is not wetted but that the galvanized steel is well wetted. However, Denkov et al [18], found a static-contact angle of deionized water to be 77.0° and 77.8°, respectively, for Perspex and galvanized steel [18]. Moreover, wall-slip velocity was found to be dependent on the liquid film's thickness [21], which is more significant for low foam qualities [7].

To our knowledge, the rheology of foam flow in capillary tubes is still debated. Diverse non-Newtonian behaviors have been observed for different experimental conditions: Newtonian, non-Newtonian shear-thinning, shear-thickening, with or without yield stress. Moreover, the impact of the tube material on the wettability, bubble size, and wall-slip velocity has not been studied in detail in previous studies. Therefore, our first objective was to investigate foam rheology in capillary tubes to better understand how foam behaves in porous media and to interpret these results both with the rheology of the same pre-generated foams flowing in porous media and the bulk foam behavior found using a rheometer. Secondly, we studied the impact of tube material and diameter on how the foam behaves in capillary tubes. We achieved these goals by experimentally investigating foam flow in different capillary tubes where foams were pre-generated through a sand-pack.

2. Theoretical considerations

The peculiarity of foam used in industrial applications is that it has a high gas fraction and a low weight compared to other liquids. A foam's characteristics change depending on the ratio of gas and liquid phases. This is generally called foam quality, and is expressed as follows

$$f_g = \frac{Q_G}{Q_G + Q_L} \quad (1)$$

where Q_G (mL/min) is the volumetric gas flow rate and Q_L (mL/min) is the volumetric liquid flow rate. The sum of both presents the total flow rate Q . The shape of the bubbles also changes with increasing foam quality, from spherical-form (wet foam, 64% < f_g < 99%) to polyhedral-form (dry foam, f_g > 99%) [40].

Darcy's law first described fluid flow through porous media with a linear relationship between the pressure gradient ∇P (Pa/m) and Darcy velocity u (m/s). It can be expressed in the following form ignoring the effects of gravity [13]

$$u = \frac{Q}{S} = -\frac{K}{\mu} \nabla P \quad (2)$$

in which K (m^2) is the intrinsic permeability, μ (Pa.s) is the dynamic fluid viscosity, Q (m^3/s), and S (m^2) the flow rate and the cross-section surface of the porous media sample, respectively. The model of a bundle of capillary tubes was also one of the first conceptual models for fluid flow in porous media. Flow in the capillary tubes was described at first by

Hagen-Poiseuille's law [59] through the relationship between the flow rate (Q , in m^3/s) and pressure drop (ΔP , in Pa). It can be presented as follows,

$$Q = \frac{\pi \Delta P R^4}{8\mu L} \quad (3)$$

where R (m) is the tube radius and L (m) is the tube length. In porous media, Kozeny [38] derived the following equation to calculate a mean pore radius R_{eq} (m) through the laws of Darcy and Poiseuille

$$R_{eq} = \sqrt{\frac{8K}{\phi}} \quad (4)$$

in which ϕ (-) is the porosity of porous media. Therefore, the wall shear rate $\dot{\gamma}$ (1/s) of a Newtonian fluid in capillary tubes can be calculated using the following equation [12],

$$\dot{\gamma} = \frac{4Q}{\pi R^3} \quad (5)$$

and the shear stress at the wall τ_w (Pa) is given by

$$\tau_w = \frac{\Delta P R}{2L} \quad (6)$$

The shear rate is not constant along the tube section and varies with the distance from the tube wall. Since foam flow through capillary tubes is primarily considered to be non-Newtonian, the Herschel-Bulkley (H-B) model [30] may be the best model to represent foam flow. It is expressed as follows

$$\mu_{app} = \frac{\tau_0}{|\dot{\gamma}|} + a|\dot{\gamma}|^{n-1} \quad (7)$$

with μ_{app} (Pa.s) being the apparent foam viscosity as a function of shear rate $\dot{\gamma}$ (1/s), τ_0 (Pa) the yield stress, a (Pa.sⁿ) consistency index, and n (-) is the flow index. If the applied stress τ is lower than τ_0 , the fluid behaves like a solid; otherwise, it flows like a fluid. The fluid can be shear-thinning for $n < 1$ or shear-thickening if $n > 1$, and is called a Bingham fluid when $n = 1$. The model reduces to the Newtonian fluid, if $\tau_0 = 0$ and $n = 1$. Therefore, the volumetric flow rate in a circular tube for Herschel-Bulkley fluids can be presented by the following relation [56]:

$$Q = \frac{8\pi}{a^{1/n}} \left(\frac{L}{\Delta P} \right)^3 (\tau_w - \tau_0)^{1+\frac{1}{n}} \left[\frac{(\tau_w - \tau_0)^2}{3 + 1/n} + \frac{2\tau_0(\tau_w - \tau_0)}{2 + 1/n} + \frac{\tau_0^2}{1 + 1/n} \right] (\tau_w > \tau_0) \quad (8)$$

which was derived through the well-known Weissenberg-Rabinowitsch equation [44,49].

Certain polymers, gels, melts, emulsions, and dispersions exhibit slipping effects on the wall of many surfaces. Due to the slip velocity, fluids may produce higher observed flow rates than flow rates due to fluidity. This phenomenon has also been observed for foams, so it is important not to ignore the slip effects at the wall when studying foam rheology [15,24,62]. The observed flow rate is the total flow rate in the tubes, which includes the foam flow rate due to fluidity and the flow rate due to the slip on the tube walls.

According to the Oldroyd-Jastrzebski correlation, the suspension flow rate through the tube of radius R in the presence of a slip effect, which is a function of shear stress, can be obtained by the following equation

$$\frac{Q_{obs}}{\pi R^3 \tau_w} = \frac{\beta}{R} + \frac{1}{\tau_w^2} \int_0^{\tau_w} \tau^2 f(\tau) d\tau \quad (9)$$

where β (-) is the slip coefficient depending on shear stress. The observed foam flow rate Q_{obs} in the capillary tubes in the presence of wall-slip effects can be expressed as:

Table 1
Sand-pack properties

Porous media	Mean grain diameter, d_{50} (mm)	Pore Volume, PV (mL)	Porosity, ϕ (%)	Permeability, K (m^2)	Mean pore radius, R_{eq} (μm)
Sand BR37	0.135	51 \pm 2	38 \pm 1	7.2 (\pm 1) $\times 10^{-12}$	11.5

Table 2
Material type and internal diameters of capillary tubes used in this study

Material	Internal diameter (mm)			
Hydrophobic	FEP	0.3 (\pm 0.01)	0.4 (\pm 0.01)	0.8 (\pm 0.01)
	PTFE	0.3 (\pm 0.01)	0.5 (\pm 0.01)	0.8 (\pm 0.01)
Hydrophilic	Glass tube (GT)	0.4 (\pm 0.01)	0.5 (\pm 0.01)	0.8 (\pm 0.01)

$$Q_{obs} = Q_f + Q_s \quad (10)$$

where Q_f (mL/min) is the foam flow rate due to fluidity corresponding to $\beta=0$. Q_s (mL/min) is the additional flow rate that occurs due to the slip effects of foam on the surface. Therefore, it can be determined as follows,

$$Q_s = \pi R^2 u_s \quad (11)$$

Wall-slip velocity u_s , must be considered on the wall since it affects flow in tubes. According to Oldroyd-Jastrzebski's method [34], the wall-slip velocity expressed by Eq. (12):

$$u_s = \tau_w \beta \quad (12)$$

The slip coefficient β ($m^2/Pa.s$) is not only defined as a function of shear stress, but it varies inversely with the tube radius. Therefore, the slip coefficient can be written in the following form:

$$\beta = \frac{\beta_c}{R} \quad (13)$$

β_c ($m/Pa.s$) is the slip correlation factor that negates the slip effect in the pipe during the flow and contributes to the foam flow rate due to fluidity. Thus, Eq. (9) can be expressed as follow, through the corrected slip coefficient that depends only on shear stress.

$$\frac{Q_{obs}}{\pi R^3 \tau_w} = \frac{\beta_c}{R^2} + \frac{1}{\tau_w^4} \int_0^{\tau_w} \tau^2 f(\tau) d\tau \quad (14)$$

3. Experimental study

This section describes the materials used, the experimental setup, and the procedures for these foam flow studies in capillary tubes.

3.2. Fluids and materials

3.1.1. Surfactant solution and gas

The surfactant solution was prepared using anionic C_{14-16} alpha-olefin sulfonate (AOS) surfactant Rhodacal® LSS-40/AX (Solvay Novcare) and demineralized water. The surfactant used was selected based on several important environmental factors such as biodegradability in soil [61,64], from field cases [60], and market availability [11]. The surfactant critical micelle concentration (CMC) was found [44] to be 1.8 \pm 0.1 g/L using a drop shape analyzer (DSA-100S, KRUSS) via the pendant-drop method [58]. The surfactant solution was prepared with four times CMC (see also [45]), which was chosen after measuring foam stability using a dynamic foam analyzer (DFA-100, KRUSS) by adopting the methodology of Yoon et al. (2019) [68].

Nitrogen gas with a purity of 99.99% was used to generate foam. It was selected after taking into account several studies in the literature on foam stability [22,69] and the solubility of gases [51]. Carbon dioxide with a purity of 99.7% was used for flushing the pre-generation column porous media during the pre-saturation procedures [1,44,45]. Air Liquide® supplied both gases.

3.1.2. Porous media and capillary tubes

Sand-pack made of calibrated silica sand (BR-37) provided by Sibelco™ was used to generate foam. The measured characteristics of the sand packing are tabulated in Table 1.

The diameters were chosen by considering the porous media in our

Table 3
Values of flow rates used in the experiment for $f_g=85\%$

Total flow rate, mL/min	Gas flow rate, mL/min	Liquid flow rate, mL/min
1.00	0.85	0.15
0.93	0.79	0.14
0.87	0.74	0.13
0.80	0.68	0.12
0.73	0.62	0.11
0.67	0.57	0.10
0.60	0.51	0.09
0.53	0.45	0.08
0.47	0.40	0.07
0.40	0.34	0.06
0.33	0.28	0.05
0.27	0.23	0.04
0.20	0.17	0.03

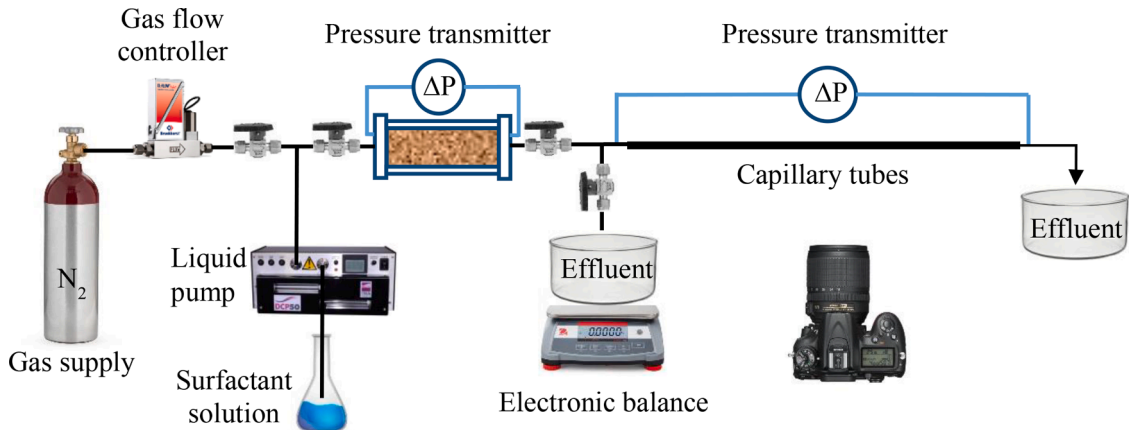


Fig. 1. Schematic of the setup used to characterize rheology in capillary tubes

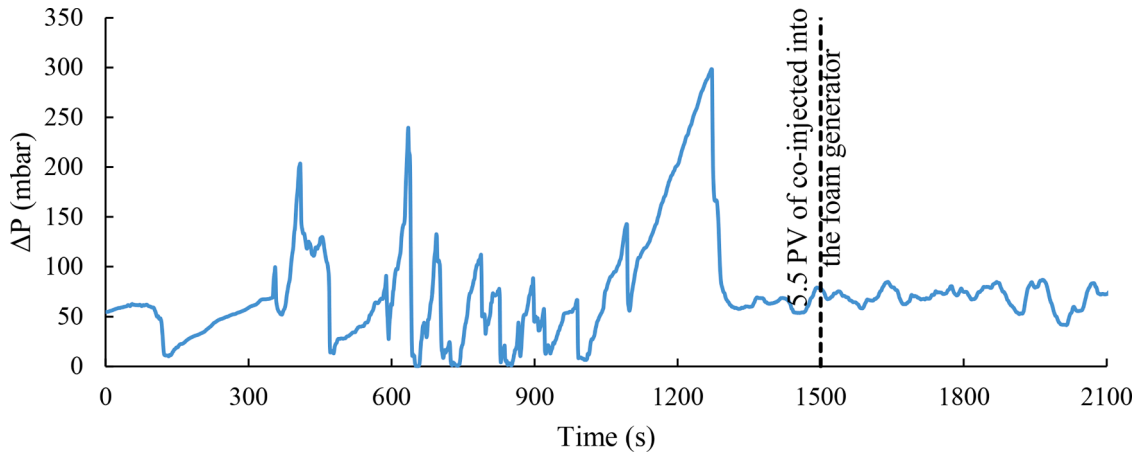


Fig. 2. Pressure difference as a function of time for $f_g=85\%$ foam in 0.8 mm diameter PTFE tube at $Q_t=1$ mL/min: the steady state occurs at 5.5 PV of foam injection in the generator

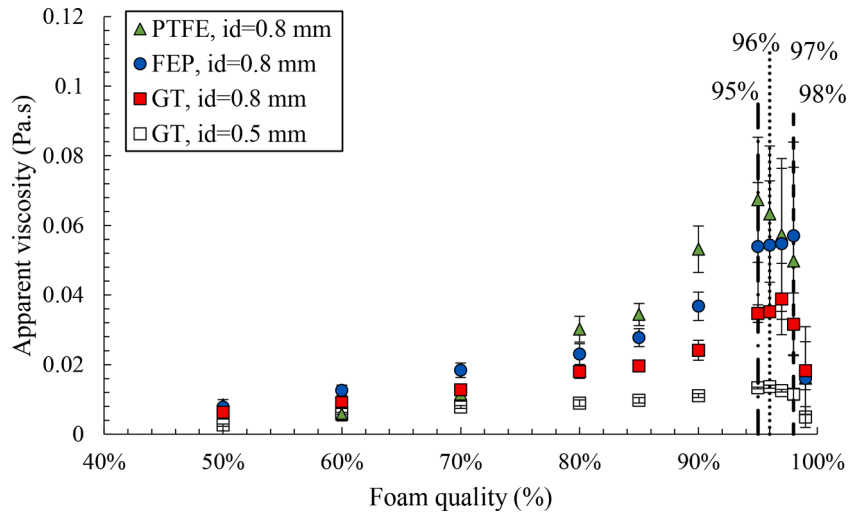


Fig. 3. Apparent foam viscosity in capillary tubes (FEP id=0.8 mm; PTFE id=0.8 mm; GT id=0.5, 0.8 mm) as a function of foam quality at $Q_t=1$ mL/min. f_g^* are shown as solid (GT, id=0.5 mm), dotted (GT, id=0.8 mm), dashed (FEP, id=0.8 mm), and dash-dotted (PTFE, id=0.8 mm) lines

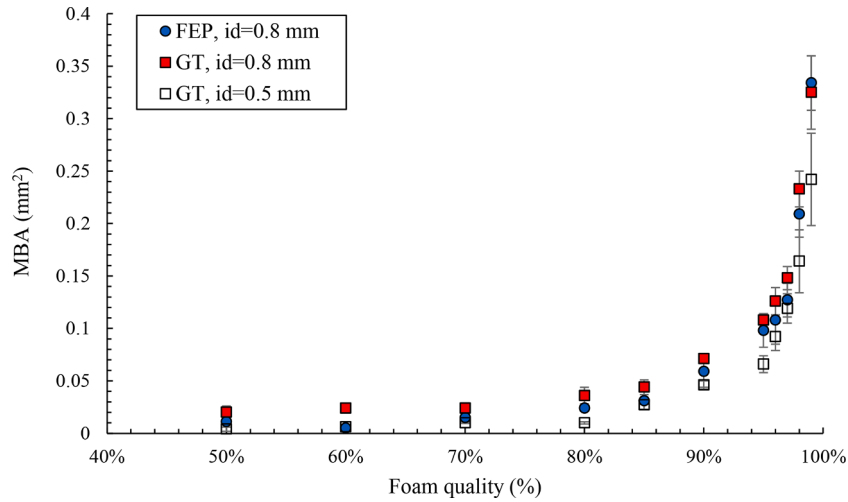


Fig. 4. Mean bubble area (MBA) as a function of foam quality in 0.8 mm FEP, 0.8 and 0.5 mm glass tubes ($Q_t=1$ mL/min)

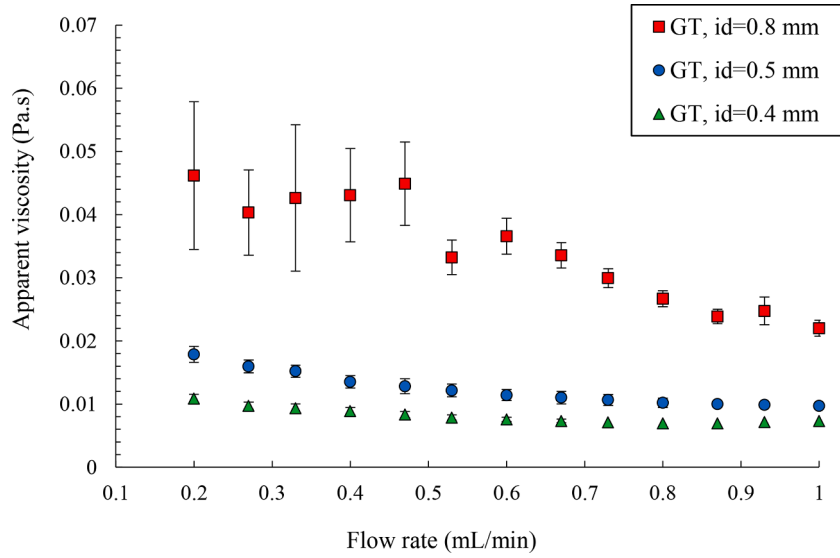


Fig. 5. Apparent viscosity as a function of total flow rate for id=0.4, 0.5 and 0.8 mm GT tubes ($f_g=85\%$)

Table 4

Fitting parameters of H-B model for FEP, PTFE, and GT tubes

Tube types id (mm)	FEP			PTFE			GT		
	0.3	0.4	0.8	0.3	0.5	0.8	0.4	0.5	0.8
n (-)	0.61 (0.27, 0.95)	0.85 (0.62, 1.08)	0.26 (-0.08, 0.59)	0.44 (-0.18, 1.07)	0.87 (0.70, 1.05)	-1.12 (-2.17, -0.05)	0.88 (0.64, 1.11)	0.63 (0.49, 0.76)	1.054 (0.28, 1.82)
τ_0 (Pa)	4.8e-05 (-7.32, 7.31)	1.61 (-0.69, 3.89)	-5.38 (-20.47, 9.72)	0.24 (-20.47, 20.96)	2.39 (1.59, 3.18)	10.28 (5.78, 14.78)	1.87 (-0.20, 3.87)	0.28 (-1.25, 1.81)	2.35 (0.96, 3.73)
a (Pa.s ⁿ)	0.11 (-0.24, 0.45)	0.02 (-0.02, 0.06)	3.24 (-6.54, 13.01)	0.46 (-2.47, 3.40)	0.02 (-0.01, 0.04)	903.9 (-268, 4495)	0.02 (-0.02, 0.05)	0.14 (-0.01, 0.28)	0.01 (-0.04, 0.06)
R^2	0.980	0.974	0.986	0.977	0.998	0.947	0.966	0.995	0.955

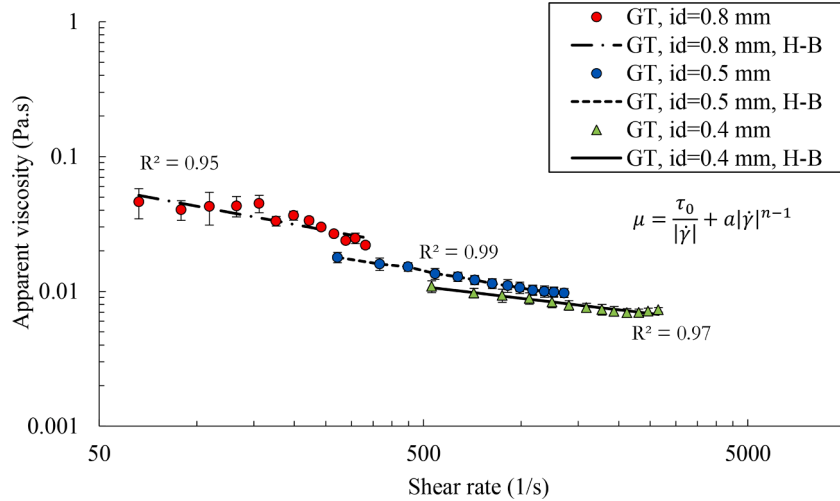


Fig. 6. Apparent foam viscosity as a function of shear rate in GT tubes with an id=0.4, 0.5, and 0.8 mm ($f_g=85\%$)

previous studies [44,45] as a bundle of capillary tubes. The mean pore radius R_{eq} of these packed column experiments was calculated using Eq. (4). We studied two types of capillary tube systems to investigate the influence of the tube material on foam property: hydrophobic systems (PTFE – polytetrafluoroethylene and FEP – fluorinated ethylene propylene) and hydrophilic (GT – smooth glass tubes). PTFE and FEP tubes were provided by Darwin microfluidics (France) and Adtech (UK), respectively. The glass tubes were obtained from DWK Life Sciences

GmbH (Germany), and the tube length was set at 40 cm. That length was selected based on the column sizes considered in our previous experiments [45]. The tube diameters were also chosen, corresponding to the permeability of glass-bead packings from the previous study [45]. Thus, according to Eq. (4), the 0.3 mm and 0.8 mm tubes represent roughly porous media with permeabilities equal to 1083 and 7700 Darcies, respectively. All capillary tubes used with their internal diameters (id) are shown in Table 2.

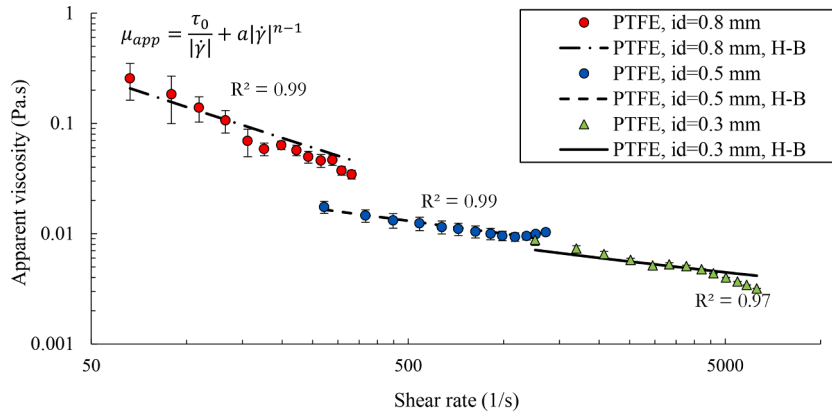


Fig. 7. Apparent foam viscosity as a function of shear rate in PTFE tubes with an id=0.3, 0.5, and 0.8 mm ($f_g=85\%$)

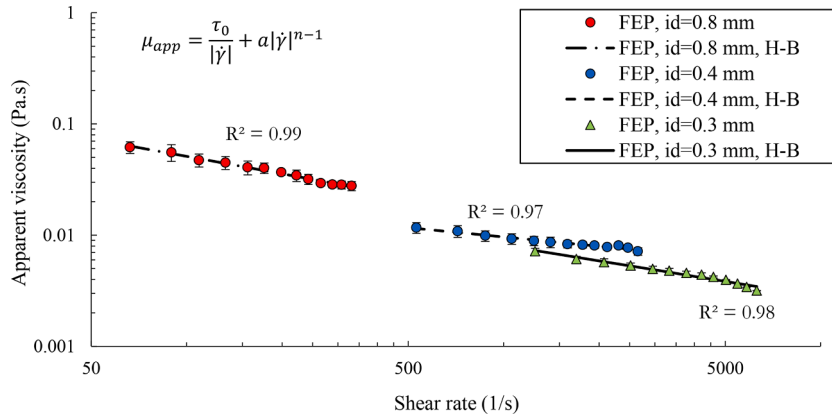


Fig. 8. Apparent foam vs. shear rate in FEP tubes with an id=0.3, 0.4, and 0.8 mm ($f_g=85\%$)

Table 5

Fitting parameters of the power-law model ($\tau_0=0$) for FEP, PTFE and GT tubes

Tube types id (mm)	FEP			PTFE			GT		
	0.3	0.4	0.8	0.3	0.5	0.8	0.4	0.5	0.8
n (-)	0.56 (0.52, 0.61)	0.72 (0.69, 0.75)	0.49 (0.45, 0.53)	0.43 (0.38, 0.49)	0.59 (0.57, 0.61)	-0.24 (-0.31, -0.18)	0.6951 (0.6617, 0.7286)	0.6052 (0.5905, 0.6199)	0.5438 (0.4945, 0.5932)
τ_0 (Pa)	0	0	0	0	0	0	0	0	0
a (Pa.s ⁿ)	0.16 (0.10, 0.22)	0.07 (0.05, 0.08)	0.54 (0.43, 0.64)	0.49 (0.28, 0.71)	0.16 (0.14, 0.18)	47.9 (34.39, 61.41)	0.07 (0.05, 0.09)	0.16 (0.15, 0.18)	0.29 (0.22, 0.37)
R^2	0.976	0.973	0.986	0.977	0.996	0.935	0.969	0.996	0.980

3.2. Experimental setup

Fig. 1 shows the experimental setup. The foam was generated by the co-injection of N_2 and the surfactant solution through the foam generator (FG). Next, the flow of pre-generated foam was studied in the capillary tubes.

The gas was supplied through the mass flow controller El-Flow Select F-201CV (Bronkhorst) with a range of 0.16-10 mL_n/min ($\pm 0.5\%$ reading, plus $\pm 0.1\%$ full scale). The surfactant solution was pumped using a DCP50 dual cylinder positive displacement pump (Strata) with $\pm 1.5\%$ setting accuracy. A foam generator column (sand-pack) made of transparent acrylic 10 cm long and with 4 cm internal diameter was used to form the foam. Two metal grids with a cell size of 42 μ m retained the sand in the column on both sides. The mass balance STX 6201 (Ohaus) was installed between the foam generator and capillary tube to record an effluent change before connecting to the capillary tubes. A Rosemount 3051S (Emerson) differential pressure transmitter in the range of

0 to 2500 mbar (± 5 mbar at the maximum value) was used to measure pressure difference along the sand-pack and capillary tubes. We studied the change in foam texture using a Nikon D850 camera (45.7 Mega Pixels) with NIKKOR LENS 105 (Nikon®). The camera was installed at the center of the tubes.

3.3. Experimental procedure

First, we thoroughly packed the foam generator column with fine sand BR37 and inspected it for leaks. Since CO_2 gas is highly soluble in water, it was used to rinse the sand-pack, thereby removing air from the porous medium. Demineralized, degassed water was injected vertically (from the column bottom) into the generator column. The injection rate was 0.5 mL/min to saturate the sand-pack by entirely dissolving CO_2 gas. The column was weighed before and after the water-saturation step to measure the pore volume (PV), i.e., the porosity. The sand-pack permeability was obtained by injecting water with different flow rates

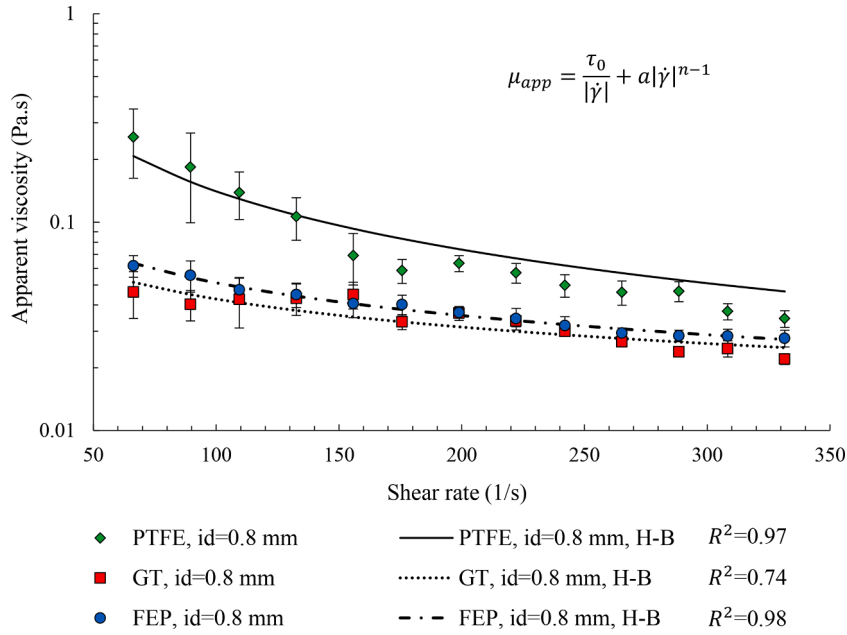


Fig. 9. Comparing apparent foam viscosities for FEP, PTFE, and GT tubes with id=0.8 mm at the same range of shear rate ($f_g=85\%$)

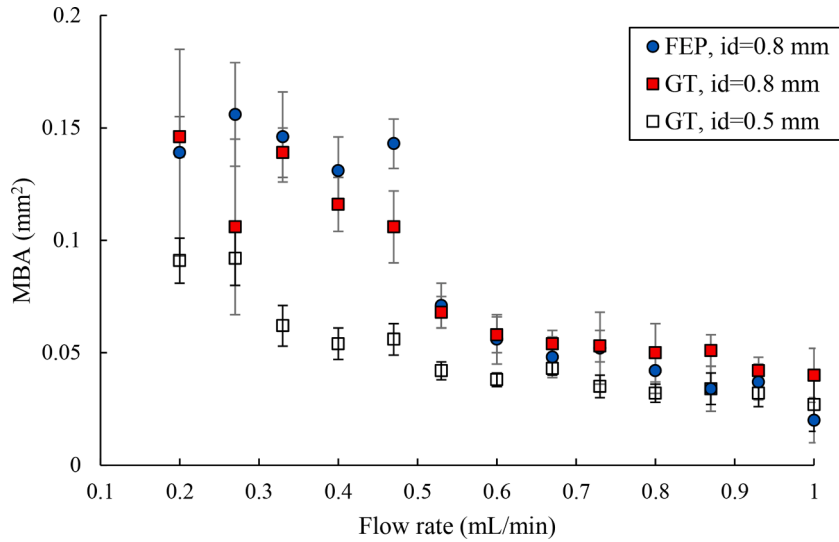


Fig. 10. MBA as a function of flow rate in 0.5 and 0.8 mm GT, and 0.8 mm FEP tubes ($f_g=85\%$)

while measuring the pressure drop along the column. The permeability of the sand-pack was calculated through Darcy's law (Eq. (2)). Then the generator column was flushed with 3 PV of the surfactant solution to satisfy the surfactant adsorption capacity of the porous medium.

In the next step, we simultaneously injected the surfactant solution and N_2 gas into the sand-pack to generate foam. The stable foam was obtained after 5 PV of fluid injection observed using the pressure transmitter data and the effluent weight. Finally, the generated foam was injected horizontally into capillary tubes. The foam flow in each capillary tube was investigated while injecting a volume equivalent to 1 PV of the foam generator by measuring the pressure drop with pressure transmitters.

To examine the impact of foam quality on foam flow behavior in capillary tubes, FEP, PTFE, and GT tubes with the same internal diameter (id= 0.8 mm) and PTFE tube with an id of 0.5 mm were studied at a fixed total flow rate of 1 mL/min while the foam quality was varied from $f_g=50\%$ to $f_g=50\%$ to $f_g=99\%$.

To study the rheology of foam in the capillary tubes, we kept the foam quality constant ($f_g=85\%$) and measured the pressure drop along the capillary tubes by adjusting the flow rates of gas and surfactant solution. The total flow rate ranged from 0.2 mL/min to 1 mL/min, as is shown in Table 3. All experiments were conducted at room temperature (20°C) and atmospheric pressure.

We also photographed foam bubbles in the 3 cm center section for each flow rate and foam quality to see the change in the foam's texture for the 0.8 mm FEP and glass tubes. The change in foam texture was not quantified in the PTFE tubes, as it was not transparent enough. ImageJ software was used to analyze the image by determining the mean bubble area (MBA). The mean area of the bubbles (as they appear against the tube wall) was estimated from 2D images taken from above of the tube wall at the 3 cm middle part. The estimations of the mean bubble area are based on the previous studies [53,63]. For instance, Tong et al [63] studied foam behavior in a vertical pseudo-2D Hele-Shaw cell. The foam bubble size distribution was estimated with image analysis using ImageJ software, measuring the cross-sectional area of each bubble (see

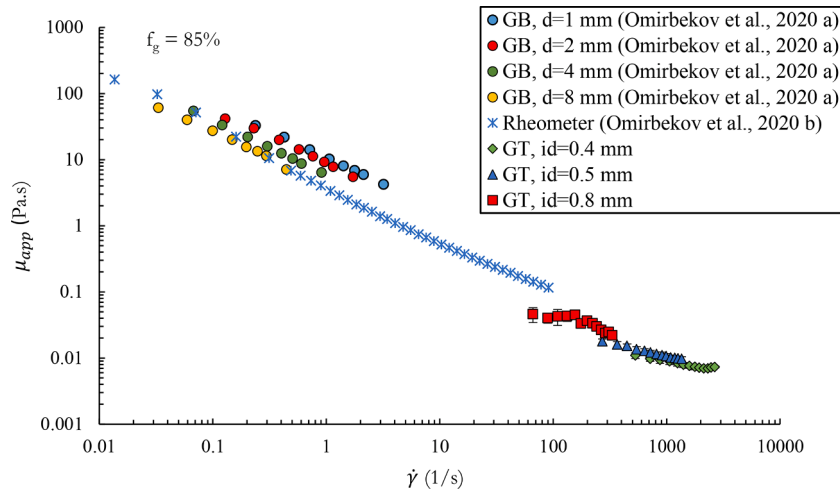


Fig. 11. Apparent foam viscosity as a function of shear rate through different methods ($f_g=85\%$): in 1 mm glass-bead packing, using a rheometer (serrated parallel-plate geometry), and in capillary tubes (GT, id=0.4, 0.5, and 0.8 mm)

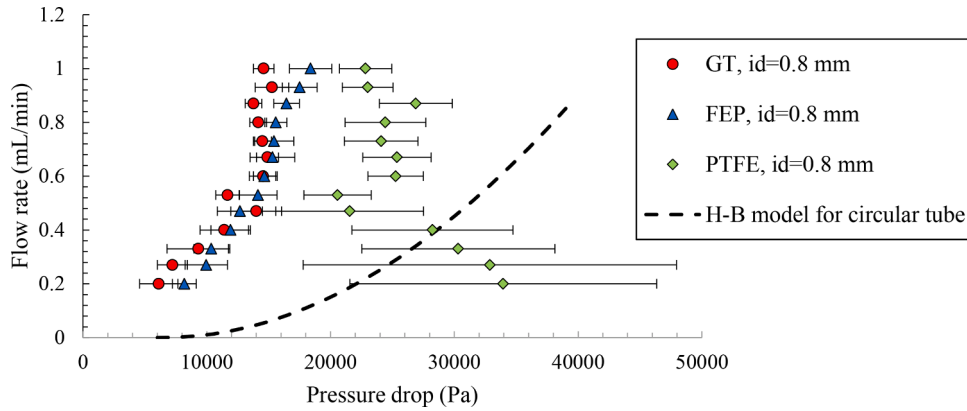


Fig. 12. Total flow rate as a function of pressure loss for GT, FEP, PTFE tubes with the id of 0.8 mm and the analytical solution for the yield-stress fluid ($f_g=85\%$)

Appendix A). According to this study, the mean bubble area is the average cross-sectional area of bubbles obtained by image analysis over a specific area in a 2D foam. Shankaran and Chinnaswamy [53] determined the size of foam bubbles to study factors controlling foamability, foam drainage, and bubble coalescence of instant coffee. The experiments were carried out in a glass column, which made it possible to capture an image of the two-dimensional structure of the foam. As in the study of Tong et al [63], Shankaran and Chinnaswamy [53] analyzed foam images in ImageJ software to determine the mean foam bubble size.

Consequently, we measured the mean area of the bubbles on 2D images of foam flow through capillary tubes. Using ImageJ's freehand selection function, we have marked all the bubbles as shown in Fig. A.1. Using the software, we measured the area of each marked bubble. After measuring all the 2D areas of the bubbles, we averaged all the results and obtained the mean bubble size. The software gave us the standard deviation and the maximum and minimum bubble areas.

4. Results and discussion

To verify the experimental configuration, we first tested the water flow at different flow rates while measuring the pressure drop along the capillary tubes. Each capillary tube was examined by the pressure sensor and compared to the results calculated using the Poiseuille equation (Eq. (3)). Results validated the setup and configuration within the pressure sensor's accuracy range.

The pre-generated foam required a particular time to achieve stabilization as the foam is not a pure single-phase fluid. 5 PV of the N_2 and surfactant solution were co-injected through the foam generator to form a stable foam. Once the foam at the generator was stable, it was connected to the capillary tube. So in the capillary tubes, the pre-generated foam had reached stabilization when a foam volume equivalent to 0.5-1 PV of the generator column had flowed through the capillary tubes. For instance,

Fig. 2 shows the $f_g=85\%$ foam-flow stability test through a 0.8 mm diameter PTFE tube for foam flow with $Q_t=1$ mL/min. The stabilization occurred after 0.5 PV (1500 s) of injection, and for lower flow rates, the stabilization time increased up to 1 PV. The average pressure drop was 70.03, with ± 8.68 mbar of oscillation because of the capillary pressure in foams. Consequently, the oscillation bars were presented by the standard deviation for each result.

4.1. Foam quality in capillary tubes: effect of tube material and bubble size

Fig. 3 shows the apparent foam viscosity as a function of foam quality for FEP, PTFE, and GT tubes with id of 0.8 mm, and GT with id=0.5 mm. The total flow rate was 1 mL/min.

The apparent foam viscosity is increased with foam quality up to a transition foam quality value (f_g^*). The domain where $f_g < f_g^*$ is the low-quality regime. The value above the transition foam quality is the high-quality regime, where the apparent foam viscosity decreases with f_g . We

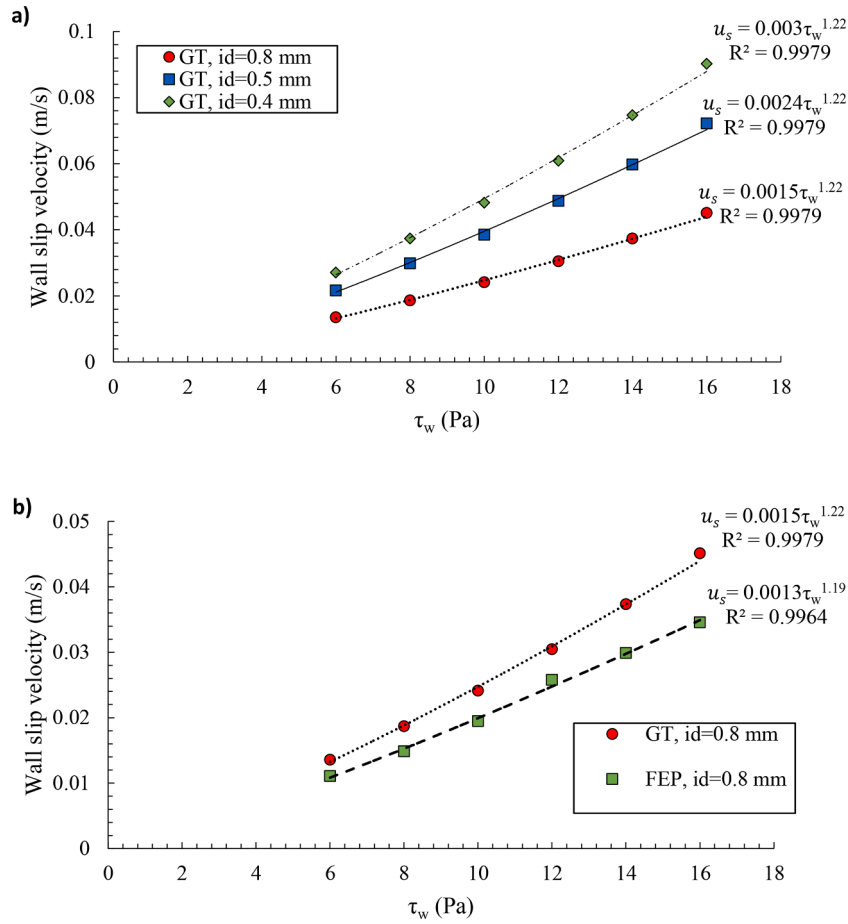


Fig. 13. Wall-shear stress vs. wall-slip velocity for a) 0.8, 0.5 and 0.4 mm GT tubes, and b) 0.8 mm GT and FEP

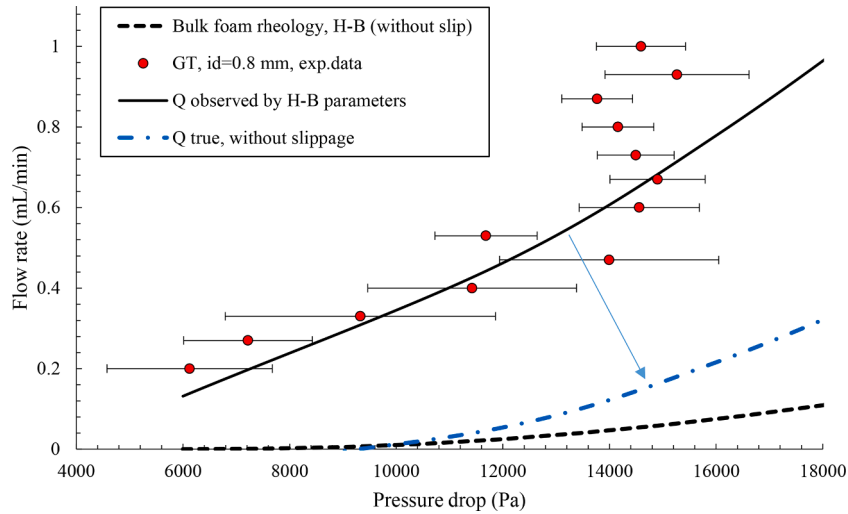


Fig. 14. Comparing the experimental data with the calculated foam flow rate values for GT tube (id=0.8 mm)

noticed that the apparent foam viscosity increased with foam quality until an instability zone occurred from $f_g^* = 95\%$, for all tubes with $id = 0.8$ mm. This instability was caused by the inter-bubble diffusion of gas from small to large bubbles, according to Fick's law. Moreover, this phenomenon became more important with the increase in foam quality. Since the Plateau borders become smaller with increasing foam quality, the gas diffusion area increases through the lamellae.

For instance, the maximum μ_{app} of foam for the FEP and PTFE were

obtained respectively at $f_g = 98\%$ (the vertical dashed line) and $f_g = 95\%$ (the vertical dash-dotted line), which corresponds to the transition foam quality f_g^* . Also, the transition foam quality f_g^* for the 0.8 mm GT was obtained at $f_g = 97\%$ (the vertical dotted line). However, the transition foam quality of 0.5 mm GT was $f_g^* = 96\%$ (the vertical solid line) against $f_g^* = 97\%$ for the same material but 0.8 mm diameter. These indicate that the transition foam quality varies depending on the material type and tube diameter.

According to the results of [45], we know that $f_g^* = 97\%$ for different glass-bead packings with monodispersed size (1 mm, 2 mm, 4 mm, and 8 mm). This confirms that f_g^* is independent of pore size for the same pre-generated foam. In their experiments, the foam-residence time (90 minutes) in the porous media, i.e., the pore volume and flow rate, were approximately identical. Therefore, the bubble size was considered to be the same if we assume that the foam bubbles coarsen at the same rate due to gas diffusion. However, the residence time was much longer than in 0.8 mm GT, around 12 s. Consequently, the bubble size tends to change less in real porous media than in capillary tubes. It is important to note that the mechanism of bubble coarsening is different in porous media experiments that occur more at high capillary pressure [36,50].

For foam flowing in tubes with the same internal diameter ($id=0.8$ mm), the viscosity was higher for the PTFE and FEP tubes than the GT: this confirms that the tube's material has an impact. The disparities observed could be attributed to the difference in wettability [48] or the effect of wall-slip velocity [31], which should be taken into account.

In Fig. 4, to observe material and tube diameter effects on bubble size, we plotted the mean bubble area (MBA) measured for each foam quality in 0.8 mm and 0.5 mm GTs, and 0.8 mm FEP tubes. Standard MBA deviation values are represented by the error bars. From the Fig., we observed exponential MBA growth with foam quality for all cases. Significantly, bubble variation was high above $f_g=90\%$. We also saw that the MBA was smaller in the FEP tube than the GT, although both tubes have the same diameter. The MBA was also smaller for the 0.5 mm GT than for the 0.8 mm GT. Since the flow rate was 1 mL/min, the velocity (i.e., shear rate) in 0.5 mm GT is about 2.5 times higher than in 0.8 mm GT. Hence, the residence time of foam in smaller tubes will be shorter and foam will undergo less coarsening.

The photos from the 0.8 mm GT are also presented in Fig. A.2 in Appendix A. From the images, we observed liquid slugs below $f_g < 70\%$, which refer to the flow of bubbly liquid. The texture of the foams between $f_g=70\%$ and $f_g=85\%$ was more homogenous, and we saw the appearance of gas slugs in the foams flowing at $f_g > 90\%$. Furthermore, these gas slugs became more substantial with increasing foam quality.

The MBA increased exponentially with foam quality, and it coarsened by two orders of magnitude at $f_g=98\%$, which corresponds to high-quality regimes according to Fig. 3. Since the plateau borders and lamellae become smaller with increasing foam quality, gas diffusion from small to giant bubbles becomes faster. Hence, we observed the flow of foam with free gas slugs (see Fig. A.2) in a high-quality regime as was indicated in the literature [23]. The pre-generated foam traveled approximately 5-25 s through the connection tubes (5 cm long, $id=1.6$ mm) between the foam generator and the capillary tubes, as the foam flow rates vary from 1.0 to 0.2 mL/min. The foam residence time in all the capillary tubes measured ($id=0.3-0.8$ mm, presented in Table 2) vary from 1.7 to 60 s at flow rates of 0.2-1 mL/min. Considering the residence time indicated above in the connecting tubes, the total residence time can vary from 6.7 to 85 s. For instance, the foam residence time in the system, including the tubes of $id=0.3$ mm, varies from 6.7 to 33.5 s when flow rates decrease from 1 to 0.2 mL/min. It is even greater for 1 mm GT, where the residence time increases from 17 to 85 s at similar flow rates of foam.

In order to better understand the gas diffusion in the tubes in relation to the residence time, we carried out a complementary experiment presented in Appendix B. However, if the MBA is roughly estimated using the calculated pore radius presented in Table 1, it will be equal to $4.15 \times 10^{-4} \text{ mm}^2$. This value is 10 times smaller than the minimum MBA shown in Fig. 4 for the 0.5 mm GT tube. The foam residence time in this experiment was 7.3 s, including 5 s in the connecting tube and 2.3 s until the middle of the 0.5 mm GT tube where the photo was taken. Based on the coarsening rate ($6.59 \times 10^{-5} \text{ mm}^2/\text{s}$) found in Appendix B, the estimated value of MBA at the outlet of foam generator is $3.52 \times 10^{-3} \text{ mm}^2$. However, it is still bigger than the calculated from the pore radius of the foam generator.

4.2. Foam rheology in capillary tubes: impact of tube diameter, material and foam texture

4.2.1. Impact of tube diameter

Fig. 5 shows the apparent foam viscosity versus the total flow rate for each GT tube at a fixed $f_g=85\%$. We found that the apparent foam viscosity in capillary tubes increases with tube diameter at the same total flow rate and decreases when the flow rate increases. This is shear-thinning foam flow behavior.

We also studied the apparent viscosity results versus the equivalent shear rate to investigate the foam rheology. The equivalent shear rates in capillary tubes were calculated from the flow rates given in Table 3 through Eq. (5). One should note that the expression of wall shear rate given in Eq. (5) has limitations for foam flow in capillary tubes according to the study of Hirasaki and Lawson [32]. In that work, the authors considered that foam flow behaves as a plug flow with slip at the wall below yield shear stress. The value of the yield stress was estimated based on the critical pressure gradient from the model developed by Princen [47].

The results show that the foam behaves as a non-Newtonian fluid. The Herschel-Bulkley model (Eq. (7)) is used to fit the experimental data, where the model parameters were estimated by nonlinear regression using the Matlab curve fitting toolbox. In the following Fig.s, the colored dots and the lines correspond respectively to the experimental data and the fitted curves using the Herschel-Bulkley model. The fitting parameters with 95% confidence intervals for each tube and the coefficient of determination are tabulated in Table 4.

Fig. 6 shows how apparent foam viscosity varies in glass tubes as a function of shear rate. From the results, we see that foam in the glass tube behaves as a shear-thinning fluid. For the 0.8 mm GT, the oscillation bars of the apparent viscosity values are relatively high compared to those at higher shear rates. This phenomenon can be explained by the transition of foam formation from weak to strong state in the generator column, which occurs when the total flow rate increases. During this process, the foam texture changes from coarse to fine, and in doing so considerably reduces gas mobility. So at low shear rates, foam flow is weak, which tends to the higher oscillations of pressure drop measurements (i.e., apparent foam viscosity). Nevertheless, we did not observe that behavior for 0.5 and 0.4 mm GTs. Almost all the results are on a trend line with slight differences due to the MBA, which can be changed with tube diameter.

Under identical conditions, the same experiments were carried out in all the FEP and PTFE capillary tubes Table 4. lists the fit curves results shown in Fig. 7 and Fig. 8 and the fitting parameters. Both Fig.s show results scattering with respect to the H-B fitting lines that increase with the tube diameter reduction. When we examine tubes with a smaller diameter, bubble size becomes more significant compared to the tube diameter because the number of bubbles decreases per tube cross-section. That causes instability in the pressure drop measurement due to the wide range of bubble size distribution along the tubes since the pressure in each bubble differs depending on its size.

Using the fitting parameters in Table 4, we observed the impact of tube diameter on foam rheology. Shear-thinning behavior was found for all tubes. The fit parameters showed the yield stress for PTFE tubes. One may observe that the estimated yield stress values increase with the diameter of the tube. Because tube experiments were conducted at certain flow rates (from 0.2 to 1 mL/min), shear rates in the 0.8 mm tube ranged from 66 to 331 1/s, while in a 0.3 mm tube, they ranged between 1257 and 6287 1/s (see Fig. 7). Since the foam in the 0.8 mm tube flowed at lower shear rates, it better predicts the yield stress according to the fitting curve. In addition, foam in these two tubes is not the same because of the longer residence time of the foam in the 0.8 mm tubes than in the 0.3 mm at the same flow rate. Moreover, the 95% confidence interval are positive for 0.5 and 0.8 mm PTFE tubes. However, the lower bound is a negative value for 0.3 mm tube since it was studied at relatively high shear rates.

From the fitting, we observed that the 95% confidence interval of the yield stress data varies from negative to positive values for both FEP and glass tubing except the 0.8 mm GT (Fig. 8). Therefore, we can conclude that the yield stress was not noticed based on the fitted curve data of GT and FEP tubes.

To ensure our statement, we fitted all the experimental data with the power-law ($\tau_0=0$) model. The fitting parameters are presented in the following table (Table 5).

From the fitting parameters of GT, we found that the power-law fits the data well, and the coefficient of determination is higher than the H-B fitting results. One should note that the H-B model included well the PTFE data, where we observed higher values of coefficient of determination that indicate a better fit for the model. Nevertheless, there is a marginal reduction in the coefficient if we exclude the yield stress in the PTFE fittings.

4.2.2. Impact of tube material

To compare the apparent foam viscosity results in tubes made of different materials, we plotted the results obtained from FEP, PTFE, and GT tubes with the same diameter in Fig. 9. At first sight, we observed that the apparent foam viscosity in hydrophobic systems (i.e., in PTFE and FEP tubes) was higher than in the glass tube, a hydrophilic material. Since the generated foam is identical, the discrepancy in fitting parameters can only be attributed to the material used for each tube. We can see that the tendency of foam flow in FEP and GT is close. However, we observe differences in the foam's apparent viscosity in the PTFE and FEP tubes, in spite of those two tubes being made of hydrophobic materials. Therefore, we found that the foam's behavior depended on material type, which may be because of wall-slip velocity.

4.2.3. Impact of foam texture

To better understand the process, we analyzed the MBA as a function of flow rates Fig. 10. shows the MBA versus flow rate for 0.8 mm and 0.5 mm GTs, and 0.8 mm FEP at foam quality of 85%. We also found that the MBA in 0.8 mm FEP is higher than 0.8 mm GT at low flow rates and becomes lower at high flow rates. The results for MBAs in the 0.8 mm GT and FEP tubes are identical within the experimental precision. That means that tube material does not significantly affect the foam texture. Changing the tube diameter does change the foam texture where the MBA is smaller. We can also see the high oscillation bars of the apparent viscosity at low flow rates, which depends on the change of foam texture with flow rates. This is obvious with all the images for 0.8 mm GT, presented in Appendix D, Fig. D.1. Notably, at low flow rates from 0.20 mL/min to 0.47 mL/min, we observed slugs of free gas that caused the large fluctuation in pressure drop measurements. As mentioned above, this phenomenon is related to the presence of weak foam, which occurs because the bubble coalescence rate is high compared to lamellae (i.e., bubble) creation in the foam generator [54].

4.3. Consistency of the foam behavior in capillary tubes with the rheology of bulk foam

To assess our results, we plotted the glass tubes result together with the outcomes of foam flow in the 1, 2, 4, and 8 mm glass bead-pack [45] and bulk foam rheology [46] in Fig. 11. The Fig. shows apparent foam viscosity vs. shear rate. In all cases, the foams were pre-generated using the same sand-pack and with a foam quality of $f_g=85\%$. These results globally show that the pre-generated foam considered here can be considered as a bulk foam if the bubbles are much smaller than the pores for the columns or much smaller than the tube diameter for the flows in capillary tubes. Although the sand pack and flow rate are the same for all data, the foam residence time, and therefore the coarsening time, differs depending on the data. However, one should note that foam flows differently in porous media than in bulk form under ambient conditions. For instance, [45] observed that the apparent foam viscosity in porous media is much higher than bulk foam viscosity and increases with the

decrease in grain size. This was an effect of compressibility that is higher in less permeable porous media [46]. Moreover, we saw that the bulk foam viscosity is higher than the apparent foam viscosity in glass tubes.

To explore this, we used the analytical expression of the Herschel-Bulkley model (Eq. (8)) for volumetric flow through the circular tubes. As input, we used the measured rheological characteristics of the bulk foam from our previous experiment [46] to study the consistency with the foam behavior in capillary tubes. When measuring the bulk foam behavior, the foam was also pre-generated using the same sand-pack. The H-B fitting parameters of bulk foam with a foam quality of $f_g=85\%$ were used in the analytical expression: $n=0.52$, $\tau_0=2.87$ and $a=0.76$.

In Fig. 12, we plotted the total flow rate versus the flow pressure drop through the 0.8 mm GT, FEP, PTFE tubes, and the H-B model's analytical solution using the bulk foam rheology. The experimental data and the analytical solution results correspond respectively to the colored dots and the dashed line in the Fig.. We found that the pressure loss in the capillary tubes is less significant than that predicted using the bulk foam rheology. This may be a consequence of wall-slip velocity in capillary tubes since the bulk foam's rheology was measured through the serrated parallel-plate geometry to eliminate the wall-slip velocity.

Since the tube diameters are the same, only surface roughness and foam wettability could affect the surface boundary condition (i.e., wall slip). Glass is a hydrophilic material with a static water-drop contact angle of 47-58° [43]; i.e., less than 90°. According to Lee et al [41]., advancing and receding water-drop contact angles on PTFE surfaces are 122° and 94°, respectively. On FEP surfaces, the values of advancing and receding contact angles are almost identical and correspond respectively to 119° and 98°. Since the surfactant solution can change the contact angle [55], the contact angle between the surfactant solution and PTFE (or FEP) can be changed [10,29]. In order to verify this, we conducted specific experiments to measure the contact angles on glass, PTFE and FEP materials (see Appendix E). We found that on PTFE and FEP surfaces, these angles are 79° and 77°, respectively. However, in Fig. 12, we can see that the results for FEP and PTFE tubes are dissimilar, and outcomes from the FEP tube are close to the smooth glass tube results. The reason for this difference is the effect of surface roughness. According to Lee et al [41]., the root-mean-square surface roughness (R_{rms}) of the PTFE and FEP materials corresponds respectively to 58.6 μm and 10.5 μm , where an atomic force microscope measured the R_{rms} on scanned areas of $10 \times 10 \mu\text{m}^2$. Therefore, the surface roughness of the PTFE material is about 6 times greater than the FEP material. Thus, we can assume that the roughness of the PTFE tubes' walls suppresses the wall-slip velocity but does not eliminate it, as was the case with the bulk foam studies by [46]. From Eq. (10), Q_{slip} was roughly estimated to be 0.19 mL/min for the 0.8 mm diameter PTFE tube. However, in the next section the wall-slip velocity is evaluated depending on the tube diameter according to [34].

4.4. Wall-slip velocity

As mentioned above, we found that the impact of tube materials on the foam rheology in capillary tubes is not negligible. Therefore, we studied the slip effects for all our tube materials following the work of Jastrzebski [34]. The Appendix D shows how we determined wall-slip velocity.

We used the same procedures to define the wall-slip effects for the FEP and PTFE tubes. However, we were unable to determine the wall effects for the outcomes of PTFE tubes because the pressure drops fluctuated greatly (see Fig. C.1). According to Fig. 12, we can confirm that the wall slip in the PTFE tube is very low or even zero. Thus, we only calculated the wall-slip velocity for GT and FEP tubes using the corrected slip coefficient, β_c Eqs. (12) and ((13)) Fig. 13. shows wall-slip velocity as a function of wall-shear stress for GT of different internal diameters (Fig. 13a), and GT and FEP of the same ($id=0.8$ mm) internal diameter (Fig. 13b).

From Fig. 13a, it is clear that the smaller the tube diameter, the higher the slip velocity at the wall (see Eq. 13). The same behavior was observed for FEP tubes (Appendix F, Fig. F.5). We found that the wall-slip velocity cannot be neglected in these tubes Fig. 11.b shows that the wall-slip velocity depends also on the material type. The wall-slip velocity was higher in GT than in FEP tubes and it increased with wall-shear stress. The results show an increase in the wall slip velocity as a function of the wall shear stress in a power-law relationship. From the foam images presented in Appendix A, Fig. A.2, we know that the foam structure at $70\% \leq f_g \leq 90\%$ is almost identical. Hence, the wall slip velocity change can be estimated using the power-law relationship presented in Fig. 13.

In Fig. 14, we again plotted the H-B model's analytical solution for circular tubes and the experimental data of 0.8 mm GT with (black solid line) and without corrected flow rates (blue dash-dotted line). The fitted curve (black solid line) that corresponds to tube experimental data is farther from the analytically obtained flow curve using bulk foam parameters. This is explained by the presence of the slip effect at the GT wall. Nevertheless, we observe the difference between the analytical solution and the flow rates due to fluidity even though the foams were pre-generated using the same sand-pack in both cases. As mentioned 4.1 section, the residence time and experimental conditions may explain this since the bulk foam was studied at ambient, open conditions [46]. showed that foam is more stable in confined media than in bulk form. (Eq.1, [6,11])

5. Conclusion

We draw these conclusions from this study:

- From experiments in capillary tubes, the apparent foam viscosity as a function of foam quality follows the classical trend globally with two regimes corresponding to the low-quality and high-quality regimes separated by a transition. However, the apparent foam viscosity increases with foam quality until instability occurs due to the texture change above $f_g=90\%$.
- For $d=0.8$ mm tubes, the transition foam quality was found to be $f_g^*=98\%$ for the FEP tube, $f_g^*=95\%$ for the PTFE tube, and $f_g^*=97\%$ for the glass tube of the same size. Thus, we can conclude that the transition quality values depend on material type. This transition foam quality is due to the gas diffusion among the bubbles that results bubble coarsening. Hence, it is different than the transition

foam quality that occurs in porous media because of high capillary pressure.

- We found the effect of material on foam flow behavior in tubes since foam behaved differently in each material with the same diameter. Moreover, better fit data was obtained if nonzero yield stress is included for foam flow data in PTFE tubes. Nevertheless, yield-stress values were found to be zero in GT and FEP tubes.
- Foam-flow imaging showed that the foam texture changes from the bubbly liquid at low foam qualities ($f_g < 70\%$) to polydisperse homogeneous foam at $70\% \leq f_g < 90\%$ and to foam with gas slugs above $f_g \geq 90\%$. The texture of the foam also changed depending on the flow rate. The foam texture was coarse at low flow rates because the weak foam was generated where the bubble coalescence rate increases compared to the bubble generation rate. Therefore, foam rheology is highly dependent on texture and bubble size.
- Foam viscosity is more significant in the PTFE tubes than the FEP and glass tubes, due to wall-slip velocity. The highest wall-slip velocity was observed in the glass tubes. However, the wall-slip velocity was higher in FEP tubes than PTFE, although both materials were hydrophobic.
- We found a change in the wettability of the PTFE and FEP materials after adding the surfactants, where the contact angle values are almost the same for the PTFE and FEP materials. Therefore, low wall-slip velocity in PTFE tubes was related to high surface roughness in the PTFE materials.

Declaration of Competing Interest

The authors declare that they have no known competing financial interests or personal relationships that could have appeared to influence the work reported in this paper.

Acknowledgments

This study was performed as part of the "Famous" project. The authors would like to thank ADEME for co-funding the project under the "GESIPOL" program and the Kazakhstan government for providing the Bolashaq International Scholarship Ph.D. grant for Sagyn Omirbekov. We gratefully acknowledge the financial support provided to the PIVOTS project by the "Région Centre – Val de Loire" and the European Regional Development Fund.

Appendix A: Measurement of the mean bubble area (MBA)

Fig. A.1 shows examples of the MBA measurement using ImageJ software. The MBA was calculated automatically by manually identifying the area of each bubble from a 2D image of the tube wall.

Fig. A.2 shows the foam texture images for each quality of foam in the glass tube. In the foams up to $f_g=70\%$, we observe liquid slugs between foams. The foam textures between $f_g=70\%$ and $f_g=85\%$ are more uniform. Above $f_g>90\%$, we observed more and bigger gas slugs as we increased the foam quality.

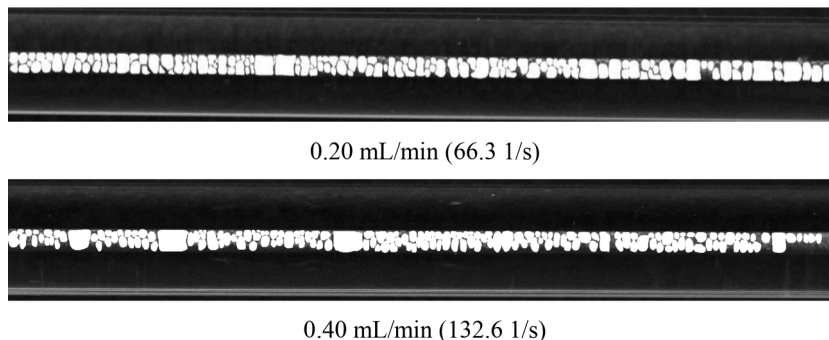


Fig. A.1. Example of the MBA determination using ImageJ

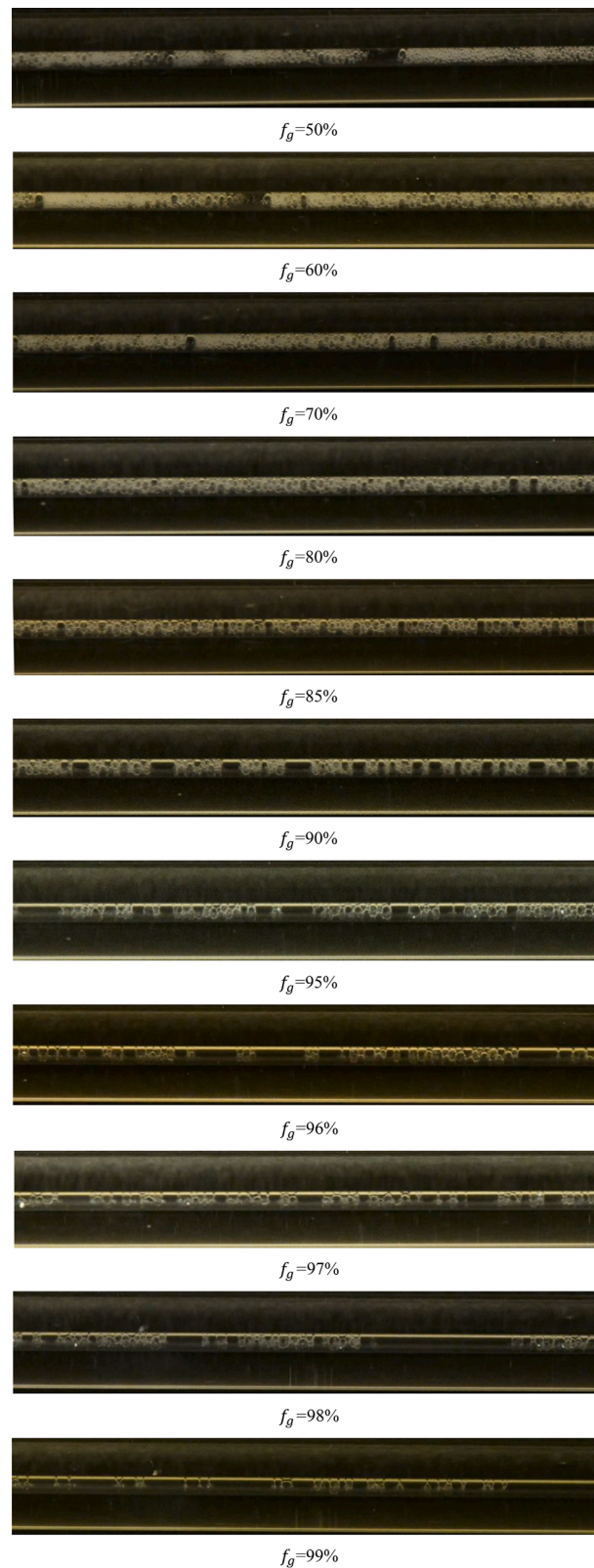


Fig. A.2. Foam images in 0.8 mm glass tube for different foam qualities ($Q_f=1$ mL/min)

Appendix B: Diffusive coarsening of foam bubbles

To study the diffusive coarsening of bubbles in tubes, the pre-generated foam from the same foam generator was introduced into a 2-meter-long PTFE tube with an inner diameter of 1.6 mm. The foam flow rate was 1 mL/min with a foam quality of 85%. The schematic of the experimental setup is shown in Fig. B.1. A Nikon D850 camera was used to capture images of the foam bubbles at various locations along the tube. The resulting images of foam bubbles were analyzed using ImageJ software.

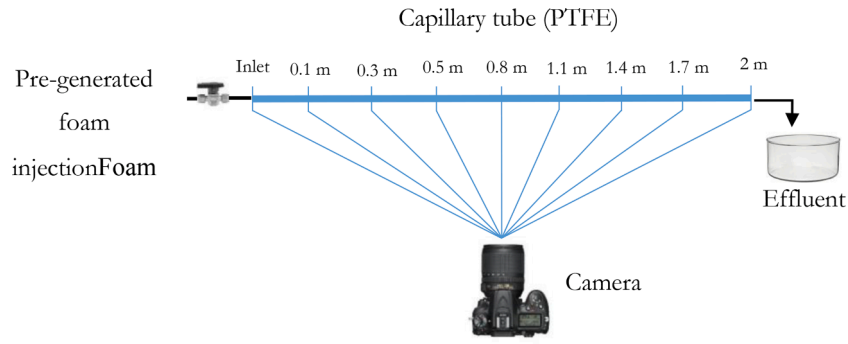


Fig. B.1. Schematic of the setup used to characterize the mean bubble area (MBA) in 1.6 mm PTFE tubes, 2 m long ($Q_t=1$ mL/min, $f_g=85\%$)

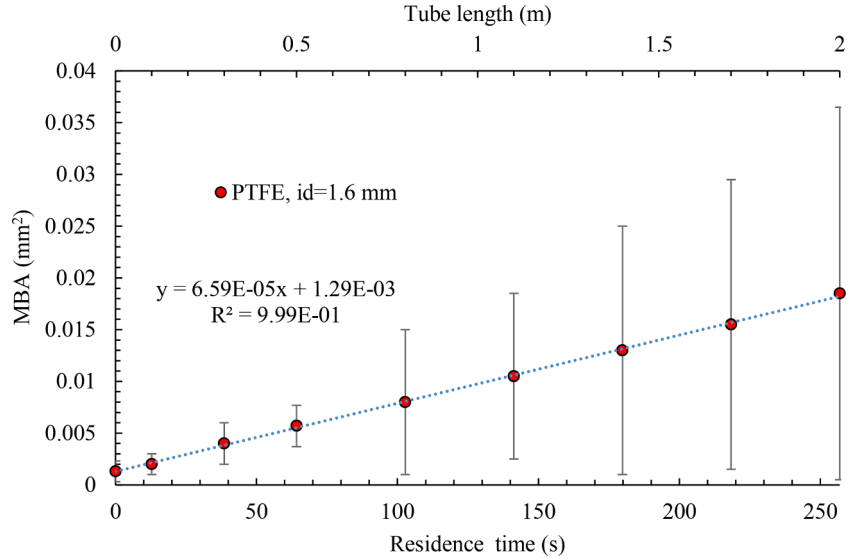


Fig. B.2. Mean bubble area (MBA) in 1.6 mm PTFE tubes 2 meters long ($Q_t=1$ mL/min, $f_g=85\%$); the bars represent the maximum and minimum bubble areas

The mean bubble area (MBA) was calculated automatically by manually identifying the area of each bubble. The internal tube volume of the 2-meter tube was 4.28 mL. Therefore, the foam residence time in the tube was 256.9 s at the flow rate of 1 mL/min. In Fig. B.2, we have plotted the change in MBA as a function of the foam residence time along the tube. The mean bubble area varies linearly as a function of residence time with a rate of 6.59×10^{-5} mm² per second. Since the residence time in the connecting tube (5 cm long, id=1.6 mm) is 5 s at the flow rate of 1 mL/min, we estimate that the MBA increased for 3.3×10^{-4} mm² ($5 \times 6.59 \times 10^{-5}$). Thus, the MBA at outlet of foam generator is 9.7×10^{-4} mm². Therefore, the MBA foam in the capillary tubes is larger than the pore size area of the foam generator (4.15×10^{-4} mm²).

Appendix C: Apparent foam viscosity in PTFE and FEP tubes

How the apparent foam viscosity in PTFE and FEP tubes varies as a function of shear rate is presented in Fig. C.1 and Fig. C.2, respectively. Both Fig. s fit well by the H-B model and show shear-thinning behavior.

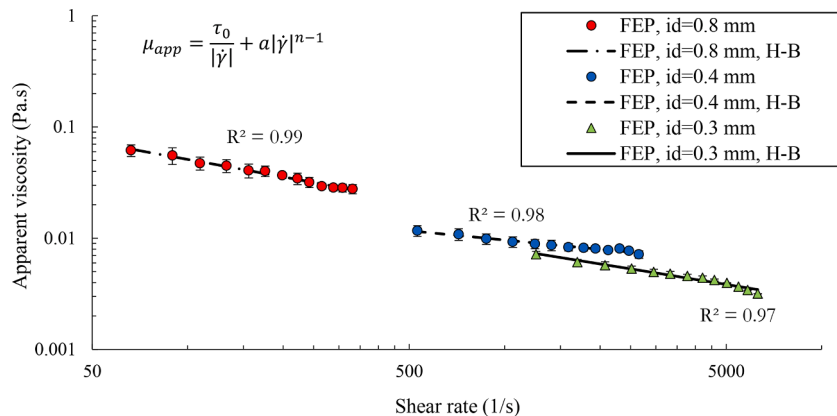


Fig. C.1. Foam images in 0.8 mm GT for different flow rates ($f_g=85\%$)

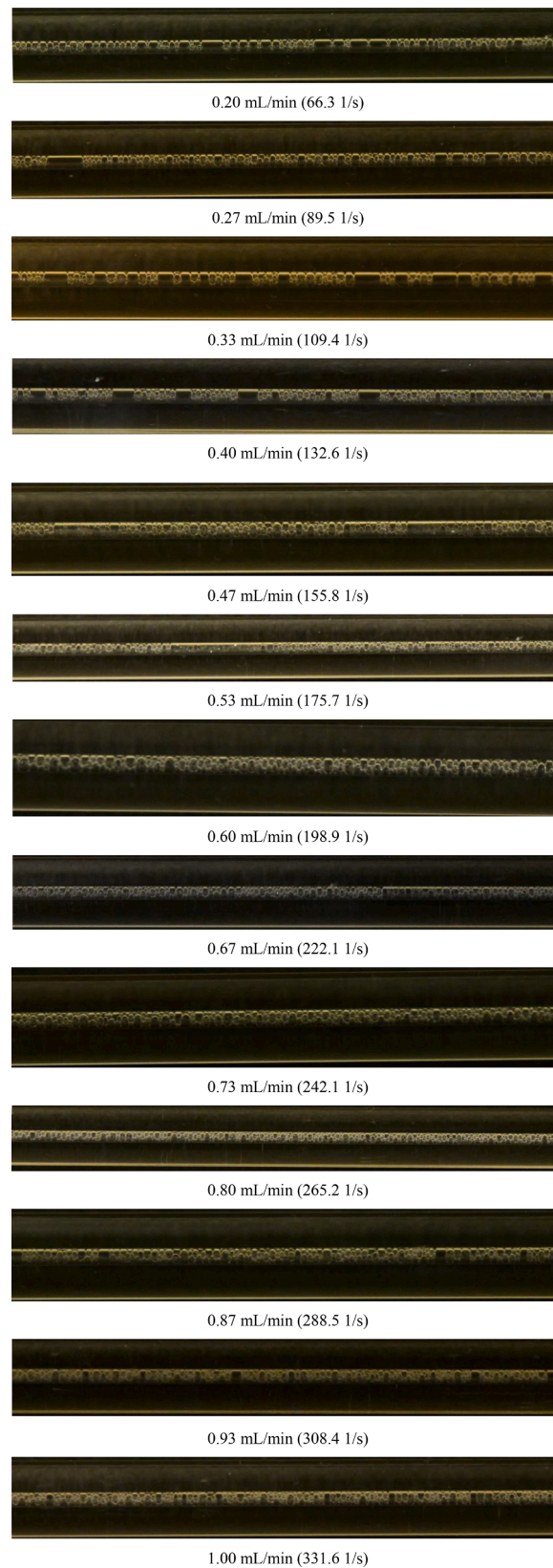


Fig. C.2. Apparent foam vs. shear rate in FEP tubes with an id=0.3, 0.4, and 0.8 mm ($f_g=85\%$)

Appendix C: Foam-flow images in 0.8 mm glass tubes versus flow rate at $f_g=85\%$



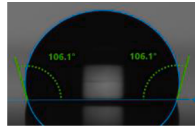

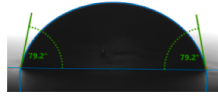
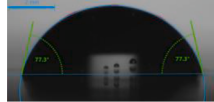
Fig. C.1 shows the photographs of steady-state foam flow in a 0.8 mm GT for flow rates in the range of 0.20 to 1 mL/min and foam quality of 85%. The images show how the high oscillation bars of the apparent viscosity depend on the change of foam texture with flow rates. At low flow rates from 0.20 mL/min to 0.47 mL/min, we observed slugs of free gas that cause large pressure-drop fluctuations.

Appendix D: Contact angle measurements on glass, PTFE, and FEP materials

The contact angles of water and the surfactant solution/nitrogen gas interface over the different materials (glass, PTFE, and FEP) plate surface was measured by the sessile drop method using a Drop Shape Analyzer (DSA-100S, KRUSS). From the results tabulated in Table D.1, we observe that PTFE and FEP are hydrophobic materials, since the measured contact angles are above 90°. However, after adding the surfactants, we found changed PTFE and FEP wettability. We found that the contact angle values are almost the same for the PTFE and FEP materials; that was around 77°.

Table D.1

The contact angle of water and the AOS surfactant solution ($4 \times \text{CMC}$)/nitrogen gas on glass, PTFE, and FEP materials

Solution	Material	Contact angle (°)
Water	Glass	 51° ± 2°
	PTFE	 110° ± 2°
	FEP	 106 ± 2°
AOS, $4 \times \text{CMC}$	Glass	 37° ± 2°
	PTFE	 79° ± 2°
	FEP	 77° ± 2°

Appendix E: Determining the wall-slip velocity

Following the method of Jastrzebski [34], we first plotted $\frac{Q_{obs}}{\pi R^3 \tau_w}$ versus τ_w in Fig. E.1 for each GT using the fitting data presented in Table 4 and Eq. (8). Then, the values of $\frac{Q_{obs}}{\pi R^3 \tau_w}$ against $1/R^2$ were replotted in Fig. E.2 to find the slopes for the specific values of shear stress τ_w . According to Eq. (14), the second term on the right-hand side represents the wall slip velocity, u_s , which is a function of shear stress (see Eqs. 12 and 13). It is obvious that if there is no-slip velocity at the wall, the slope will be zero. Therefore, the corrected slip coefficient β_c was obtained as the slopes from a graph of $\frac{Q_{obs}}{\pi R^3 \tau_w}$ versus $\frac{1}{R^2}$. The corrected slip coefficient increases with increasing wall shear stress.

The same procedures were used to define the wall-slip effects for the FEP and PTFE tubes. The results for FEP tubes were also presented in Fig. E.3 and Fig. E.4. However, we were unable to determine the wall effects for the outcomes of PTFE tubes due to the high fluctuation in the pressure drop results. Therefore, we could not produce slopes from the $\frac{Q_{obs}}{\pi R^3 \tau_w}$ versus $\frac{1}{R^2}$ graph and we only calculated the wall-slip velocity for GT and FEP tubes using the corrected slip coefficient β_c Eqs. (12) and ((13)) Fig. E.5. shows the results of wall-shear stress vs. wall-slip velocity for 0.8, 0.4, and 0.3 mm FEP tubes. As expected from Eq. (13), the smaller the tube diameter, the higher the slip velocity at the wall.

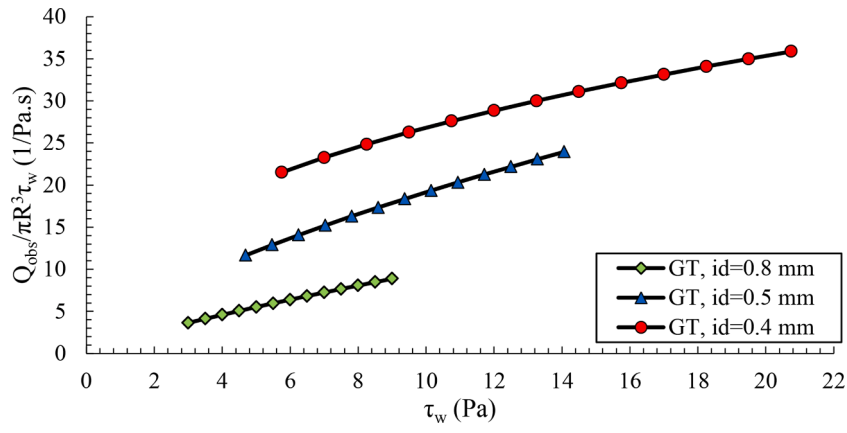


Fig. E.1. $Q_{obs}/\pi R^3 \tau_w$ vs. τ_w for 0.4, 0.5, and 0.8 mm GT tubes

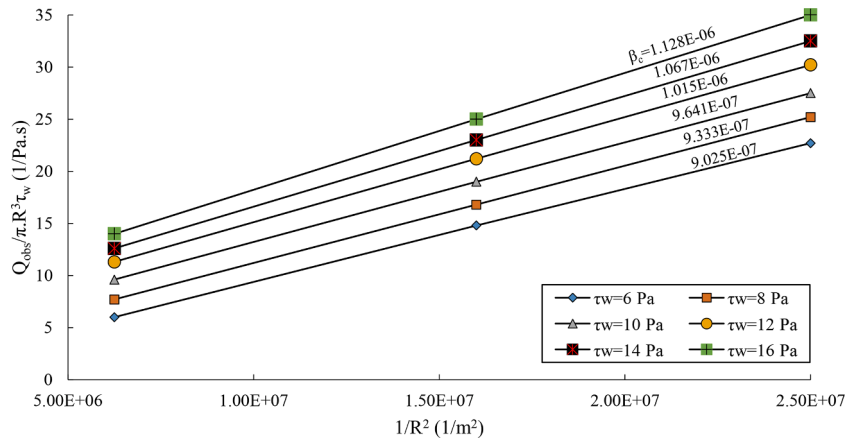


Fig. E.2. Corrected slip coefficients for GT tubes from slopes of lines obtained by plotting $Q_{obs}/\pi R^3 \tau_w$ vs. $1/R^2$ with τ_w as a parameter

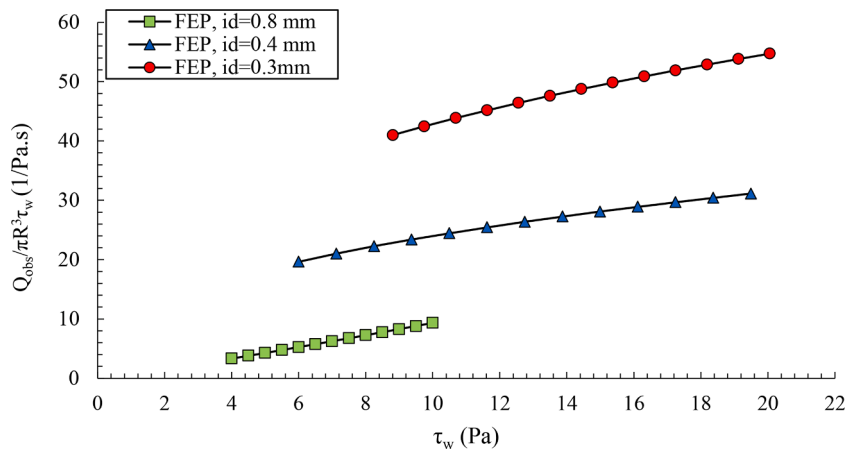


Fig. E.3. $Q_{obs}/\pi R^3 \tau_w$ vs. τ_w for 0.4, 0.5, and 0.8 mm FEP tubes

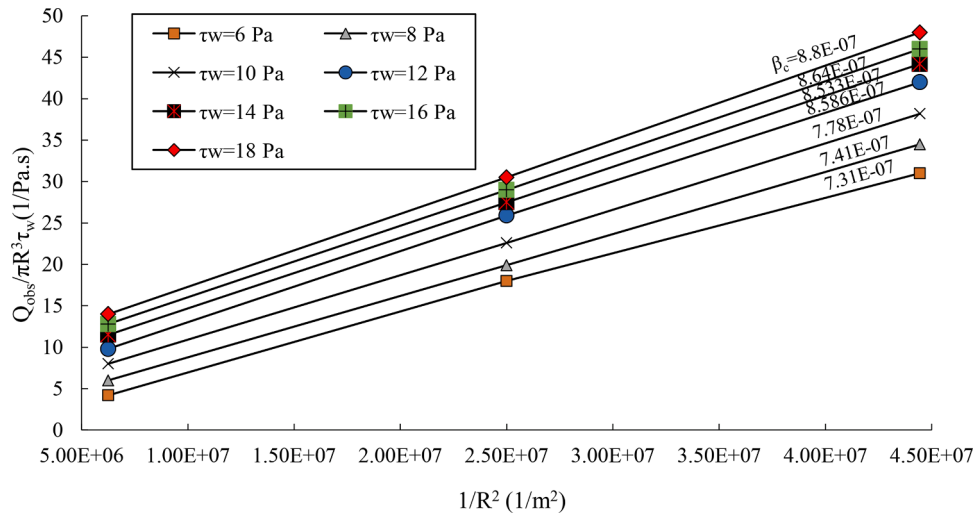


Fig. E.4. Corrected slip coefficients for FEP tubes from slopes of lines obtained by plotting $Q_{obs}/\pi R^3 \tau_w$ vs. $1/R^2$ with τ_w as a parameter

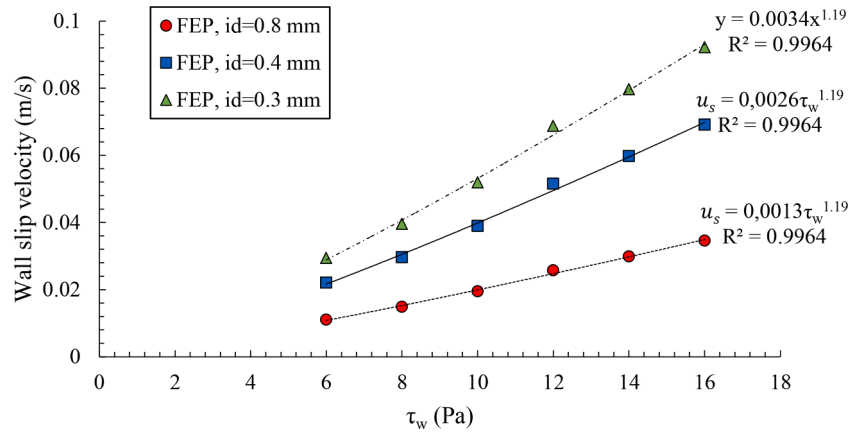


Fig. E.5. Wall-shear stress vs. wall-slip velocity for 0.8, 0.4 and 0.3 mm FEP tubes

References

- [1] R. Aranda, et al., Experimental study of foam flow in highly permeable porous media for soil remediation, *Transp. Porous Media* 134 (2020) 231–247.
- [2] A.G. Ardakani, et al., Monitoring polymer-enhanced foam displacements through heterogeneous porous media: a pore-scale study, *J. Energy Res. Technol.* 142 (2020).
- [3] H. Bertin, E.D.C. Estrada, O. Atteia, Foam placement for soil remediation, *Environ. Chem.* (14) (2017) 338–343.
- [4] M. Bogdanovic, R.N. Gajbhiye, S.I. Kam, Experimental study of foam flow in horizontal pipes: two flow regimes and its implications, *Colloids Surf. A* 344 (2009) 56–71.
- [5] F.P. Bretherton, The motion of long bubbles in tubes, *J. Fluid Mech.* (10) (1961) 166–188.
- [6] R. Burley, M. Shakaran, Experimental study of foam rheology in straight capillary tubes, *Int. J. Eng. Fluid Mech.* (5) (1992) 115–141.
- [7] J.R. Calvert, K. Nezhati, A rheological model for a liquid-gas foam, *Int. J. Heat Fluid Flow* 7 (1986) 164–168.
- [8] I. Cantat, N. Kern, R. Delannay, Dissipation in foam flowing through narrow channels, *EPL* (65) (2004) 726.
- [9] A.R. Castro, M. Oostrom, N. Shokri, Effects of shear-thinning fluids on residual oil formation in microfluidic pore networks, *J. Colloid Interface Sci.* 472 (2016) 34–43.
- [10] R.G. Chaudhuri, S. Paria, Dynamic contact angles on PTFE surface by aqueous surfactant solution in the absence and presence of electrolytes, *J. Colloid Interface Sci.* 337 (2009) 555–562.
- [11] T. Cserhádi, E. Forgács, G. Oros, Biological activity and environmental impact of anionic surfactants, *Environ. Int.* 28 (2002) 337–348.
- [12] R. Darby, R. Darby, R.P. Chhabra, *Chemical Engineering Fluid Mechanics, Revised and Expanded*, CRC Press, 2001 s.l.
- [13] H.P.G. Darcy, *Les Fontaines Publiques de la Ville de Dijon. Exposition et Application des Principes à Suivre et des Formules à Employer Dans les Questions de Distribution D'eau*, etc, V. Dalamont, 1856 s.l.
- [14] H. Davarzani, et al., Experimental study of foam propagation and stability in highly permeable porous media under lateral water flow: diverting groundwater for application to soil remediation, *J. Contam. Hydrol.* 243 (2021), 103917.
- [15] David, A., Marsden Jr, S. S. & others, 1969. *Rheology of foam*, s.l., s.n.
- [16] N.D. Denkov, V. Subramanian, D. Gurovich, A. Lips, Wall slip and viscous dissipation in sheared foams: Effect of surface mobility, *Colloids Surf. A* 263 (2005) 129–145.
- [17] N.D. Denkov, et al., The role of surfactant type and bubble surface mobility in foam rheology, *Soft Matter* (5) (2009) 3389–3408.
- [18] N.D. Denkov, S.S. Tcholakova, R. Höhler, S. Cohen-Addad, Foam rheology, in: P. Stevenson (Ed.), *Foam Engineering: Fundamentals and Applications*, John Wiley & Sons, Ltd, 2012 s.l.
- [19] Du, D. X., Li, Y. G. & Sun, S. J., 2011. Experimental study on pseudo-plastic behavior for film foam flow in a vertical tube, s.l., s.n., p. 194–199.
- [20] F.A.L. Dullien, *Porous Media: Fluid Transport and Pore Structure*, Academic press, 1992 s.l.
- [21] C. Enzendorfer, et al., Pipe viscometry of foams, *J. Rheol.* 39 (1995) 345–358.
- [22] R. Farajzadeh, A. Andrianov, H. Bruining, P.L.J. Zitha, Comparative study of CO₂ and N₂ foams in porous media at low and high pressure–temperatures, *Ind. Eng. Chem. Res.* 48 (2009) 4542–4552.
- [23] R.N. Gajbhiye, S.I. Kam, Characterization of foam flow in horizontal pipes by using two-flow-regime concept, *Chem. Eng. Sci.* 66 (2011) 1536–1549.
- [24] B.S. Gardiner, B.Z. Dlugogorski, G.J. Jameson, Rheology of fire-fighting foams, *Fire Saf. J.* 31 (1998) 61–75.
- [25] B.S. Gardiner, B.Z. Dlugogorski, G.J. Jameson, Prediction of pressure losses in pipe flow of aqueous foams, *Ind. Eng. Chem. Res.* 38 (1999) 1099–1106.
- [26] A. Gumati, H. Takahshi, Experimental study and modeling of pressure loss for foam-cuttings mixture flow in horizontal pipe, *J. Hydrodyn. Ser. B* (23) (2011) 431–438.
- [27] P.C. Harris, Effects of texture on rheology of foam fracturing fluids, *SPE Prod. Eng.* 4 (1989) 249–257.
- [28] P.C. Harris, V.G. Reidenbach, others, High-temperature rheological study of foam fracturing fluids, *J. Petroleum Technol.* 39 (1987) 613–619.

- [29] F. Henrich, et al., Influence of surfactants in forced dynamic dewetting, *Soft Matter* 12 (2016) 7782–7791.
- [30] W.H. Herschel, R. Bulkley, Konsistenzmessungen von gummi-benzollösungen, *Kolloid-Zeitschrift* 39 (1926) 291–300.
- [31] B. Herzhaft, S. Kakadjian, M. Moan, Measurement and modeling of the flow behavior of aqueous foams using a recirculating pipe rheometer, *Colloids Surf. A* 263 (2005) 153–164.
- [32] G.J. Hirasaki, J.B. Lawson, Mechanisms of foam flow in porous media: apparent viscosity in smooth capillaries, *Soc. Pet. Eng. J.* 25 (1985) 176–190.
- [33] G.J. Hirasaki, et al., Surfactant/Foam Process for Aquifer Remediation, Society of Petroleum Engineers, 1997, p. 1.
- [34] Z.D. Jastrzebski, Entrance effects and wall effects in an extrusion rheometer during flow of concentrated suspensions, *Ind. Eng. Chem. Fundam.* (6) (1967) 445–454.
- [35] S.A. Khan, C.A. Schnepfer, R.C. Armstrong, Foam rheology: III. Measurement of shear flow properties, *J. Rheol.* 32 (1988) 69–92.
- [36] Z.I. Khatib, G.J. Hirasaki, A.H. Falls, others, Effects of capillary pressure on coalescence and phase mobilities in foams flowing through porous media, *SPE Reservoir Eng.* 3 (1988) 919–926.
- [37] A.R. Kovscek, C.J. Radke, Fundamentals of foam transport in porous media, *ACS Adv. Chem.* 55 Series 242 (1994) 115–164.
- [38] J. Kozeny, Über kapillare leitung der wasser in boden, *Royal Acad. Sci., Vienna, Proc. Class I* 136 (1927) 271–306.
- [39] L.W. Lake, *Enhanced Oil Recovery*, Prentice Hall, 1989 s.l.
- [40] D. Langevin, Aqueous foams and foam films stabilised by surfactants. Gravity-free studies, *Comptes Rendus Mécanique* 345 (2017) 47–55.
- [41] S. Lee, J.-S. Park, T.R. Lee, The wettability of fluoropolymer surfaces: influence of surface dipoles, *Langmuir* 24 (2008) 4817–4826.
- [42] J. Maire, H. Davarzani, S. Colombano, N. Fatin-Rouge, Targeted delivery of hydrogen for the bioremediation of aquifers contaminated by dissolved chlorinated compounds, *Environ. Pollut.* 249 (2019) 443–452.
- [43] S. Mitra, et al., Interaction dynamics of a spherical particle with a suspended liquid film, *AlChE J.* 62 (2016) 295–314.
- [44] M. Mooney, Explicit formulas for slip and fluidity, *J. Rheol.* (1929-1932) (2) (1931) 210–222.
- [45] S. Omirbekov, H. Davarzani, A. Ahmadi-Senichault, Experimental study of non-newtonian behavior of foam flow in highly permeable porous media, *Ind. Eng. Chem. Res.* 59 (2020) 12568–12579.
- [46] S. Omirbekov, H. Davarzani, S. Colombano, A. Ahmadi-Senichault, Experimental and numerical upscaling of foam flow in highly permeable porous media, *Adv. Water Res.* (2020), 103761.
- [47] H.M. Princen, Rheology of foams and highly concentrated emulsions: I. Elastic properties and yield stress of a cylindrical model system, *J. Colloid Interface Sci.* 91 (1983) 160–175.
- [48] H. Qi, et al., Effect of pipe surface wettability on flow slip property, *Ind. Eng. Chem. Res.* 57 (2018) 12543–12550.
- [49] B. Rabinowitsch, Über die viskosität und elastizität von solen, *Zeitschrift für physikalische Chemie* 145 (1929) 1–26.
- [50] W.R. Rossen, M.W. Wang, Modeling foams for acid diversion, *SPE J.* (4) (1999) 92–100.
- [51] R. Sander, Compilation of Henry's Law Constants For Inorganic and Organic Species of Potential Importance In Environmental Chemistry, Max-Planck Institute of Chemistry, Air Chemistry Department Mainz, Germany, 1999 s.l.
- [52] A.E. Scheidegger, *The Physics of Flow Through Porous Media*, University of Toronto, Toronto, 1974.
- [53] P.I. Shankaran, A. Chinnaswamy, Instant coffee foam: An investigation on factors controlling foamability, foam drainage, coalescence, and disproportionation, *J. Food Process Eng.* 42 (2019) e13173.
- [54] J.J. Sheng, *Enhanced Oil Recovery Field Case Studies*, Gulf Professional Publishing, 2013 s.l.
- [55] R. Singh, K.K. Mohanty, Foams with wettability-altering capabilities for oil-wet carbonates: a synergistic approach, *SPE J.* 21 (2016) 1–126.
- [56] A.H.P. Skelland, *Non-Newtonian Flow and Heat Transfer (Book on Quantitative Relationships for Non-Newtonian Systems, Considering Classification and Fluid Behavior of Materials with Anomalous Flow Properties)*, 1967, JOHN WILEY AND SONS, INC., NEW YORK, 1967, p. 469.
- [57] T. Sochi, M.J. Blunt, Pore-scale network modeling of Ellis and Herschel–Bulkley fluids, *J. Pet. Sci. Eng.* 60 (2008) 105–124.
- [58] C.E. Stauffer, The measurement of surface tension by the pendant drop technique, *J. Phys. Chem.* 69 (1965) 1933–1938.
- [59] S.P. Sutera, R. Skalak, The history of Poiseuille's law, *Annu. Rev. Fluid Mech.* 25 (1993) 1–20.
- [60] M. Svab, M. Kubal, M. Müllerova, R. Raschman, Soil flushing by surfactant solution: pilot-scale demonstration of complete technology, *J. Hazard. Mater.* (163) (2009) 410–417.
- [61] S.S. Talmage, *Environmental and Human Safety of Major Surfactants: Alcohol Ethoxylates and Alkylphenol Ethoxylates*, CRC Press, 1994 s.l.
- [62] N.N. Thondavadi, R. Lemlich, Flow properties of foam with and without solid particles, *Ind. Eng. Chem. Process Des. Dev.* 24 (1985) 748–753.
- [63] M. Tong, K. Cole, S.J. Neethling, Drainage and stability of 2D foams: foam behaviour in vertical Hele-Shaw cells, *Colloids Surf. A* 382 (2011) 42–49.
- [64] M.E. Tuvell, et al., AOS — An anionic surfactant system: Its manufacture, composition, properties, and potential application, *J. Am. Oil Chem. Soc.*, 01 1 55 (1978) 70–80.
- [65] P.W. Voorhees, The theory of Ostwald ripening, *J. Stat. Phys.* 38 (1985) 231–252.
- [66] S. Wang, C.N. Mulligan, An evaluation of surfactant foam technology in remediation of contaminated soil, *Chemosphere* 57 (2004) 1079–1089.
- [67] Q. Xiong, T.G. Baychev, A.P. Jivkov, Review of pore network modelling of porous media: experimental characterisations, network constructions and applications to reactive transport, *J. Contam. Hydrol.* 192 (2016) 101–117.
- [68] I.-H. Yoon, S.B. Yoon, C.-H. Jung, C. Kim, S. Kim, J.-K. Moon, W.-K. Choi, A highly efficient decontamination foam stabilized by well-dispersed mesoporous silica nanoparticles, *Colloids Surf. A* 560 (2019) 164–170.
- [69] Y. Zeng, et al., Role of gas type on foam transport in porous media, *Langmuir* 32 (2016) 6239–6245.